

UNIVERSIDAD DE LAS PALMAS DE GRAN CANARIA
Máster Oficial en Sistemas Inteligentes y Aplicaciones Numéricas en Ingeniería



Trabajo Final de Master

**Numerical and computational implementation of
physical interaction processes between particle
beams and plasmas.**

Pablo Rodríguez Beltrán

Tutores: José María Escobar Sanchez
Juan Miguel Gil de la Fe

Fecha: 3 de Septiembre de 2018

Abstract

This work belongs to the framework of the interaction between an ion beam and a plasma target, which is one of the main lines of work in the area of inertial confinement nuclear fusion, as this one of the best candidates to operate the ignition of a future confinement nuclear fusion power plant. Thereby, the simulation of the beam-plasma interaction process is necessary to obtain information about the energy deposition of the beam particles in the plasma. In this work, we propose a physical and numerical model to study the energy loss of the beam and the heating of the plasma, where both processes depend on the stopping power magnitude, which accounts the deceleration of the projectiles in the plasma. The physical and numerical models have been implemented in a computational code called STOPBIN, which simulates the beam-plasma interaction process. Thus, the spatial and temporal solutions of the stopping power, the energy of the beam and the temperature of the plasma are obtained. The results of the simulation are compared with the researches of other authors under different conditions and physical parameters. Once the validity of the model is checked, we propose a set of experiments in order to illustrate the capabilities of the model: first, it is studied the interaction between a proton beam and an Aluminum plasma, in standard conditions of laboratory experiments; secondly, it is simulated the interaction between a proton beam and a Deuterium-Tritium plasma, which is usually studied for the fast ignition of a nuclear fusion process. Finally, the results of this simulations are analyzed, the main conclusions of the work and a brief description of future lines of work are presented.

Contents

Abstract	i
1 Introduction	1
1.1 Background Work	2
1.2 Objectives	3
1.3 Work Structure	4
2 Physical Model	5
2.1 Theoretical Background	5
2.2 Beam-Plasma Interaction	7
2.2.1 Beam-Plasma Hamiltonian	7
2.2.2 Dynamic Equations of the System	7
2.2.3 Energy Loss and Stopping Power Definition	9
2.2.4 Stopping Power Expressions of the Model	10
2.3 Heating of the Plasma	12
2.4 Atomic Kinetic Equations Plasma	14
2.5 Summary of the Physical Model	16
3 Numerical and Computational Models	17
3.1 Numerical Approaches to the problem	17
3.1.1 Euler method	17
3.1.2 Runge Kutta method	18
3.1.3 Error Estimation	18
3.1.4 Adaptive Mesh	19
3.2 Discretization of the Physical Model	20
3.2.1 Discretization of the Plasma and the Energy Loss	20
3.2.2 Discretization of the Temperature Equation	22
3.2.3 Summary of the Discrete Problem	23
3.3 MIXKIP Code	24
3.4 Computational Implementation: STOPBIN	26
3.4.1 Additional Features	28
4 Simulation and Results	33
4.1 Simulation Test	33
4.1.1 Numerical Model Test	33
4.1.2 Adaptive Mesh	35
4.2 Behavior and Comparative with other models	36

4.3 Experiments	40
4.3.1 Proton Beam in an Aluminum Plasma	41
4.3.2 Proton Beam in a Deuterium-Tritium Plasma	49
5 Conclusions	53
5.1 Future Lines of Work	54

Chapter 1

Introduction

Studying the physical properties of matter has been one of the most important fields of physics in the last centuries. Gas, liquid and solid states are the most familiar kinds of matter, but since the second half of the XX century a lot of effort has been employed in the study of the plasma state.

Plasma state is compound by both neutral (atoms, molecules, neutrons, photons...) and charged components (ions, free electrons, protons...). Unlike the other three states, plasma does not exist freely on the Earth's surface under normal conditions, so it can only be artificially generated by heating or applying a strong electromagnetic field. In the nature, plasma is mostly associated with stellar interiors and atmospheres, the rarefied intracuster medium and possibly in the intergalactic regions. Moreover, matter in plasma state can be generated in laboratories or in nuclear fusion facilities.

In figure 1.1 there is a graph where the different kinds of a plasma are displayed depending on its temperature and the free electron density. This figure proves the wide range of plasmas that are found in the nature and can be studied, as its properties can vary significantly.

Fundamental research and modeling in plasma atomic physics, like radiative properties and particle and laser beams-plasma interaction, continues to be essential for providing basic understanding and advancing on many different topics relevant to high-energy-density systems, particularly for nuclear fusion and astrophysics plasmas.

Thus, in the field of inertial confinement fusion the radiative properties are the responsible of the absorption by the dopants in the fuel ablator of the thermal radiation in the indirect drive scheme.

On the other hand, beam-plasma interaction experiments are one of the key tools to investigate the physics properties of matter under extreme conditions, like high-energy-density plasmas. A detailed theoretical description of the interactions allows us to diagnose the temperature and density, obtain information about the dynamic structure function, opacities and the equation of state of the plasmas.

This beam-plasma interaction is essential in the inertial confinement nuclear fusion research area, as it is expected to be one of the best candidates to operate the ignition of a future confinement fusion power plant, where a precise knowledge of the energy deposition of the beam particles is required to design the fusion process.

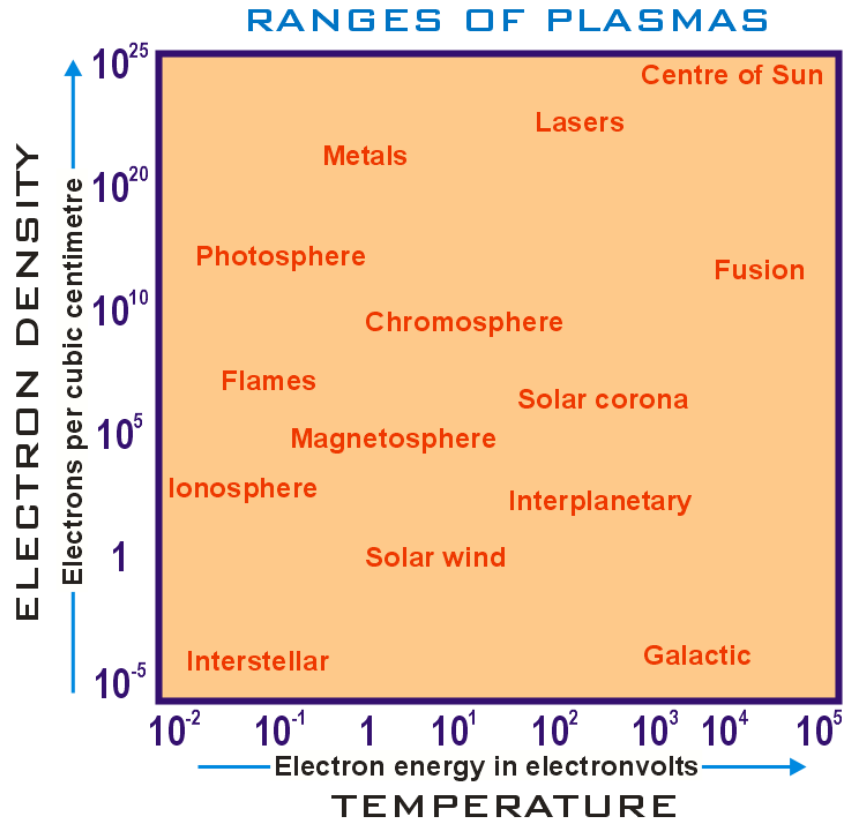


Figure 1.1: Graph showing the classification of a plasma depending on its temperature and free electron density, [1].

Also, the researches in beam-plasma interactions are essential for providing basic understanding of some astrophysics problems. Thus, the plasma emissivity is a key quantity in the structure, behavior and stability of radiative shock waves which are presented in many astrophysical scenarios. Therefore, the plasma properties are essential to analyze and explain both experiments and observations and also the radiative-hydrodynamics numerical simulations.

1.1 Background Work

This TFM (Trabajo de Fin de Master) has been developed under the idea of mixing the computational and numerical knowledge acquired during the Master SIANI (Sistemas Inteligentes y Aplicaciones Numericas en la Ingeniería) course with the researches of the GIRMA group. GIRMA (Grupo de Interacción Radiación MAteria) is a research group with members from the Physic Department of the ULPGC (Universidad de las Palmas de Gran Canaria) and from the Plasma Atomic Physics Section of the IFN-UPM (Instituto de Fusión Nuclear de la Universidad Politécnica de Madrid).

GIRMA has a long experience in the study and development of theoretical and computational models, as well as simulations of various processes of plasma physics. The ongoing research of GIRMA focuses on the implementation of numerical mod-

els in computational codes intended to simulate the atomic structure and atomic kinetics of plasma, aiming to obtain the abundances or populations of the charge and quantum states present in the plasma, as well as its radiative properties. Therefore, these studies serve as a framework for the development of the contents of the Master SIANI, in particular learning Fortran, Matlab and various computational calculation methods with engineering applications.

This work leans on one of the codes created by GIRMA, MIXKIP, that will be necessary to calculate some data, so studying its code structure is considered as a part of the TFM duties, therefore there will be an explanation of the operation of this code in future chapters. Moreover, the code developed in this TFM, called STOPBIN, will ultimately complement MIXKIP code.

1.2 Objectives

This work focuses on developing a theoretical and computational model for the simulation of the stopping of a point-like ion beam in a high energy density plasma, as well as the plasma heating process in a wide range of conditions. Space-time dependence simulations of the beam-plasma interaction for different conditions are presented, paying special attention to the stopping power, the energy loss of the beam, the range of the ion beam in the plasma and the change of the temperature field in the heating process.

The main objectives of this work, synthesized in a few points are:

- The introduction to the concepts and basic equations of the plasma physics and ion beam-plasma interaction processes.
- The development of a physical-numerical model for the study of the interaction of the ion beam with the plasma.
- The implementation of the proposed physical and numerical model in the computational code STOPBIN, that will complement MIXKIP code.
- The simulation of the ion beam-plasma interaction processes in different physical situations, using STOPBIN code.

On the other hand, the didactic content of this work will teach the physical concepts that explain the interaction between a beam and a plasma, the methodology to model a physical system, the numerical techniques and computational capabilities that the simulation uses and will improve the skill to handle programming languages such as *Fortran* and *Matlab*.

1.3 Work Structure

This document is organized as follows: first, in this chapter is found a brief introduction to plasmas as the fourth state of matter, the state of the art and its applications; in the second chapter the plasma basic models are explained, the physical model is built using the ideas of the previous chapter, including the expressions that will be used to simulate the ion-plasma interaction; then, the numerical model selected to solve the model is explained in the third chapter; in the fourth chapter the model is tested, compared with other models and the results of our own experiments are shown; in the last chapter, the main conclusions of this TFM and some future lines of work are explained. Finally, there will be an Appendix with a proposed extension of the MIXKIP code.

Chapter 2

Physical Model

This chapter collects the physical foundations to describe a beam-plasma interaction, which is the main subject of this work. First, the concept of plasma is introduced, as well as the basic considerations and equations to treat it. Then the interaction between the plasma and the beam is studied, the beam behavior is described and it is proposed a set of equations that govern the whole system, in order to built the model that will be simulated in the next chapter. That is, the equation of the stopping power of the plasma and the equations that govern the changes of the kinetic energy of the beam and the temperature of the plasma.

2.1 Theoretical Background

As it is explain in the Introduction, a plasma is compound by neutral particles (atoms, molecules, neutrons, photons, etc) and charged components (ions, electrons, protons, etc), where collective effects i.e, large range interaction effects, are important. In order to analyze a plasma from a physical point of view, it needs to be studied from a microscopic and macroscopic perspective.

The microscopic description involves:

- The study of the internal atomic structure, in particular the energy levels and wave functions of the ions under the influence of the surrounding plasma. So, the Dirac equation is solved in a quantum relativistic scenario or the Schrödinger equation in a non relativistic one.
- The analysis of the collisional and radiative processes occurred in the plasma, such as the ionizations caused by electron/ions impacts or the excitation of an ion by absorption of a photon, among others. This implies calculating the cross sections (probabilities) and rates (number of processes per time) for each possible process.
- A study of the populations of the different components of the plasma. Atomic kinetic transport or collisional-radiative equations are applied to calculate the space-time distribution of the ion and atoms populations both for each charge state, ground and excited configurations. Moreover, the radiative transport equations are applied to calculate the energy distribution for the photons.

A macroscopic description involves:

- The study of the radiative properties of the plasma, from the magnitudes determined in the microscopic description.
- An analysis of the state equations of the plasma as a function of the temperature and density, using statistical physics.
- It is studied the space-time evolution of some fields, such as temperature, density, pressure, etc, under initial and boundary conditions. Fluid mechanics are applied among the hydrodynamics equations in interaction with electromagnetic radiation.

All the previous points show the wide complexity of this problem. Moreover, some of the equations mentioned above are coupled because the system is compound of a huge number of particles that interact with each others. So, the simulations of plasma properties at high energy density require the development of complex theoretical models and their computational implementation for the generation of large plasma properties databases in a wide range of plasma conditions. These plasma properties involve the calculation of a huge number of atomic levels (around 10^5) and atomic processes (around 10^7). It is also necessary, to solve a very large set of coupled rate equations to obtain the average ionization of the plasma and the populations of the atomic levels. Moreover, this set must be solved for each plasma condition, i.e. density and temperature, the system must be resolved, and in a hydrodynamic simulation the profile of plasma conditions could involve around 10^3 of them. Therefore, it is necessary to use some approximations to uncouple this equations.

GIRMA research group tackle this problem separating it in two steps. First, the microscopic equations are solved and then, its solutions are applied to the calculations of the radiative properties of the plasma. The MIXKIP code mentioned in the previous chapter 1, is used in this work to characterize the plasma, as its physical model will be explained in section 2.4 and its computational structure will be presented in the future chapter, in the section 3.3.

2.2 Beam-Plasma Interaction

This section contains a physical description of the projectile-target system. First, it will be presented the hamiltonian of the system, which governs the dynamic evolution of its particles. Secondly, some appropriate approaches to the dynamic model are explained, in order to choose a proper description of the system. Then, there are presented the expressions that govern the interaction between the beam and the previously explained plasma, as the behavior of both in time and space.

2.2.1 Beam-Plasma Hamiltonian

The starting point to model and simulate the interaction between a plasma and an ion beam (considering a single projectile) is the hamiltonian of the system. This hamiltonian is compound by a plasma target term H_T , a non relativistic projectile term H_P and the its projectile-target interaction V_{P-T} , which is switched at a certain time with a step function ($\theta(t - t_0)$). The hamiltonian is written as:

$$H = H_T + H_P + \theta(t - t_0) \cdot V_{P-T}(\vec{\mathbf{R}}, \{\vec{\mathbf{S}}, \vec{\mathbf{s}}, \vec{\mathbf{s}}\}) \quad (2.1)$$

$$H_P = \frac{\mathbf{P}^2}{2m_P}; \quad H_T = H_{CM} + H_{bound} + H_{free} + H_{int};$$

Where $\vec{\mathbf{R}}$, $\vec{\mathbf{P}}$ and m_P are the position, the momentum and the mass of the projectile respectively, t_0 is the instant when the interaction begins.

The hamiltonian of the target plasma H_T is split in four parts: the first two terms represent each ion system, which is divided in its mass center (usually approached as the nucleus) and the bound electrons per each ion; the third term represents the free electrons of the plasma; the fourth term takes into account the interaction between the other three hamiltonians. Thus, the plasma coordinates $\{\vec{\mathbf{S}}, \vec{\mathbf{s}}, \vec{\mathbf{s}}\} = \{\vec{\mathbf{S}}_1 \dots \vec{\mathbf{S}}_{N_i}; \vec{\mathbf{s}}_{1,1} \dots \vec{\mathbf{s}}_{1,N_{b,i}} \dots \vec{\mathbf{s}}_{N_i,1} \dots \vec{\mathbf{s}}_{N_i,N_{b,i}}; \vec{\mathbf{s}}_1 \dots \vec{\mathbf{s}}_{N_e}\}$ can be associated to the ions mass centers, the bound electron of this ions (position respect to its mass center) and the coordinates of the free electrons, respectively. Furthermore, N_i is the number of ions in the plasma, $N_{b,j}$ is the number of bound electrons of the j^{th} ion and N_e is the number of free electrons.

2.2.2 Dynamic Equations of the System

Once the hamiltonian has been introduced, the purpose of this section is to find approach to describe the dynamic of the system. Because of the large number of components of the plasma, the problem is highly complex, so there are different possible approximations to solve the 2.1 hamiltonian.

On one hand, the hamiltonian could be treated in a molecular dynamic context, i.e, solving the newtonian or hamiltonian equations of each component of the plasma and the beam simultaneously, as the equations are coupled due to the interactions. In this description, the dynamic equations of the i^{th} component of the system (either the ions of the beam, ions of the plasma or the free electrons) are given in the

hamiltonian formalism by:

$$\dot{\vec{r}}_i = \frac{\partial H}{\partial \vec{p}_i}; \quad \dot{\vec{p}}_i = -\frac{\partial H}{\partial \vec{r}_i} \quad (2.2)$$

Or, in the newtonian formalism by:

$$\vec{F}_i = \frac{d\vec{p}_i}{dt}; \quad \vec{V}_i = \frac{d\vec{r}_i}{dt}; \quad (2.3)$$

Where \vec{r}_i and \vec{p}_i are the position and momentum either for beam or plasma particles, where \vec{F}_i represents the force over the i^{th} component due to the interaction with the rest of particles of the system. This is a very detailed description in time and space for each component, however it requires an enormous computational cost, due to the great number of coupled equations to solve.

On the other hand, an alternative consist in using a statistical description, which consist in solving the Liouville equation of the system. Thereby, it is possible to derive, from the hamiltonian 2.1, the probability density $\rho(\{\vec{r}, \vec{p}\}, t)$ in the phase space $\{\vec{r}, \vec{p}\}$ of the system. Thus, in a statistical context, the average of a magnitude $A(\{\vec{r}, \vec{p}\}, t)$ in a volume Ω of the phase space, could be calculated as:

$$\langle A \rangle_{\{\vec{r}, \vec{p}\}} = \int_{\Omega} d\vec{r}_1 \dots d\vec{r}_n d\vec{p}_1 \dots d\vec{p}_n dt \rho(\{\vec{r}, \vec{p}\}, t) A(\{\vec{r}, \vec{p}\}, t); \quad (d\vec{r} = d^3r) \quad (2.4)$$

Expression 2.4 can be expressed in terms of the distribution function in the phase space of one particle, $f(\vec{r}, \vec{p}, t)$, and it is defined as the integral of $\rho(\{\vec{r}, \vec{p}\}, t)$ over all the coordinates except one. It can be also determined in an approximated way when is calculated from the kinetic or Boltzmann equations, where the correlations between three or more particles are despised. In the last case, the average of a magnitude could be calculated as:

$$\langle A \rangle_{\vec{r}, \vec{p}} = \int_{\Omega} d\vec{r} d\vec{p} dt f(\vec{r}, \vec{p}, t) A(\vec{r}, \vec{p}, t) \quad (2.5)$$

Once several descriptions have been explained, it is possible to choose different treatments for each component of the system, which, as the hamiltonian shows, is compound by the projectile, the plasma components and its interaction.

In this work, we focus in analyzing the dynamic of the ion beam within the plasma. We will study the projectile under a classical deterministic dynamic description in the newtonian formalism. Moreover, it is considered that the particles of the beam do not interact with each other, and therefore, its behavior is ruled by its interaction with the plasma particles. This interaction yields a force ($F_{T-P} = \vec{F}_i$) from the plasma over the projectile i^{th} , given by:

$$F_{T-P} \equiv \vec{F}_i = -\vec{\nabla} V_i, \quad \text{with } V_i = \sum_j V_{T-P_{ij}} \quad (2.6)$$

Being $V_{T-P_{ij}}$ the potential that suffers the particle i^{th} of the ion beam, due to its interaction with a j^{th} particle of the plasma.

In our model, this force is considered an statistical average over the plasma coordinates, in the context of the expression 2.5, but in the phase space of the plasma. With this description for the problem all the contributions of the plasma components to the interaction are averaged and large computational works are avoided.

In the study of the dynamic of the projectile we will center in the change in its kinetic energy as it dives in the plasma, as it will be seen in the next section, the variation of this energy is related with the averaged force previously commented.

2.2.3 Energy Loss and Stopping Power Definition

In the experiments that explore the interaction between an ion beam and a plasma, the ion projectiles lose its energy gradually as they dig in the target plasma. Considering a point-like projectile (internal structure is despised), a key observable to quantify is the kinetic energy loss ΔEk of the projectile, which difference is empirically determined by comparing the energy of the projectile before and after passing through the plasma.

A much more detailed magnitude to measure is the stopping power Sp , defined as the energy loss of the projectile per path-length unit:

$$\frac{dEk}{ds} = -Sp \quad (2.7)$$

If the projectile has sufficiently high kinetic energy and/or mass, it can be considered that travels along a straight line. For low energies the projectile shows a Brownian motion with stochastically changing momentum, so in the trajectory will appear transverse and longitudinal fluctuations which are defined as spreading and straggling respectively. In this work the beam will have enough energy to consider that the movement of the projectiles across the plasma is straight and the problem is one-dimensional. Under this approximations the stopping power can be described as:

$$\frac{dEk}{dx} = -Sp = -\frac{\vec{V}}{V} \cdot \vec{F}_{T-P} \quad (2.8)$$

Where \vec{F}_{T-P} represents the decelerating force that the ion suffers due to the interaction with the plasma in a ds space region, as it was explained in the end of the previous section 2.2.2. Also, \vec{V} is the velocity of the projectile before entering the ds region.

The most general expression for the stopping power has a dependence in its projectile and plasma set of coordinates and momentums.

$$Sp(\vec{\mathbf{R}}, \vec{\mathbf{P}}, \{\vec{\mathbf{r}}, \vec{\mathbf{p}}\}, t) = \frac{\vec{V}(t)}{V(t)} \cdot \vec{F}_{T-P}(\vec{\mathbf{R}}, \vec{\mathbf{P}}, \{\vec{\mathbf{r}}, \vec{\mathbf{p}}\}, t) \quad (2.9)$$

Where $\{\vec{\mathbf{r}}\} = \{\vec{S}, \vec{s}, \vec{s}\}$ represents the coordinates of each particle of the plasma and $\{\vec{\mathbf{p}}\}$ are its associated momentum. Also, $\vec{\mathbf{R}}$ and $\vec{\mathbf{P}}$ is the coordinate and momentum of the projectile.

However, as it is explained in the previous section 2.2.2, the projectile will be consider under a classical deterministic approximation, so both projectile coordi-

nates and momentum will be time dependent ($\vec{\mathbf{R}}(t), \vec{\mathbf{P}}(t)$) and expression 2.9 can be rewritten as:

$$Sp(\{\vec{\mathbf{r}}, \vec{\mathbf{p}}\}, t) = \frac{\vec{V}(t)}{V(t)} \cdot \vec{F}_{T-P}(\{\vec{\mathbf{r}}, \vec{\mathbf{p}}\}, t) \quad (2.10)$$

This expression provides the stopping of the projectile in a t instant, when it has a V speed and the plasma is in the $\{\vec{\mathbf{r}}, \vec{\mathbf{p}}\}$ state. Now, our interest is to express the stopping power as a magnitude where the plasma variables have been averaged, as it is pointed in the previous section 2.2.2. Thereby, the stopping power in a t instant where the plasma parameters are averaged over $\{\vec{\mathbf{r}}, \vec{\mathbf{p}}\}$, is given by:

$$Sp(t) = \langle Sp(\{\vec{\mathbf{r}}, \vec{\mathbf{p}}\}, t) \rangle_{\{\vec{\mathbf{r}}, \vec{\mathbf{p}}\}} = \frac{\vec{V}(t)}{V(t)} \cdot \left\langle \vec{F}_{T-P}(\{\vec{\mathbf{r}}, \vec{\mathbf{p}}\}, t) \right\rangle_{\{\vec{\mathbf{r}}, \vec{\mathbf{p}}\}} \quad (2.11)$$

Finally, applying the expression 2.5 to calculate 2.11, we can find the desired average over all the plasma:

$$Sp(t) = \frac{\vec{V}(t)}{V(t)} \cdot \int_V d\vec{r}_1 \dots d\vec{r}_n \int_0^\infty d\vec{p}_1 \dots d\vec{p}_n f(\{\vec{\mathbf{r}}, \vec{\mathbf{p}}\}, t) \vec{F}_{T-P}(\{\vec{\mathbf{r}}, \vec{\mathbf{p}}\}, t) \quad (2.12)$$

After averaging over the plasma coordinates, the stopping power will have a parametric dependence on certain macroscopic parameters that represent the averaged plasma: $Sp(t) = Sp(t; n_{ef}, n_a, T)$, where n_{ef} is the free electron density, n_a is the atomic density and T is the temperature of the plasma. This procedure is used to find the expressions of the stopping of the beam with free electrons, bound electrons and ions. A great number of stopping power models have been proposed in the last decades under different approximations [2, 3, 4, 5]. The free electrons and ion stopping will be consider under a classical context, while bound electrons stopping is obtained in a quantum formalism, as it is explained in the coming section 2.2.4.

2.2.4 Stopping Power Expressions of the Model

In this work the stopping power of the ion projectile is considered to be the sum of the stopping with the target free electrons, the target bound electrons and the target ions (mass centers) [6].

$$Sp = Sp_{free} + Sp_{ion} + Sp_{bound} \quad (2.13)$$

The Sp_{free} and Sp_{ion} are calculated by using the Peter and Meyer-ter-Vehn (PMV) model [7]. This stopping power model was develop in a classical statistic context, in the framework of the kinetic theory. In our work we use the analytical approximation of the PMV model, as it is shown below for both free electrons and ions:

Free electron stopping, shows the contributions of the free electrons to the stopping power, valid when $Z_P/(n_{ef}\lambda_{De}^3) < 1$:

$$Sp_{free}(V, T, n_{ef}) = \frac{Z_P^2 e^4}{4\pi\epsilon_0^2 m_e} \cdot \frac{n_{ef}}{V^2} \cdot (G_e \cdot L_e + H_e \cdot \log(X_e)), \quad \text{with :} \quad (2.14)$$

$$\begin{aligned}
X_e &= V/V_e \\
L_e &= \log(\lambda_{D_e}/b_e) \\
G_e &= \operatorname{erf}(X_e/\sqrt{2}) - \sqrt{2/\pi} \cdot X_e \cdot e^{-(X_e^2)/2} \\
H_e &= (-X_e^3 \cdot e^{-(X_e^2)/2})/(3\sqrt{2\pi}) + X_e^4/(X_e^4 + 12)
\end{aligned}$$

Ion electron stopping, shows the contributions of the mass centers of the atoms to the stopping power, valid when $Z_P/(n_a \lambda_{D_i}^3) < 1$:

$$S_{p_{ion}}(V, T, n_{at}) = \frac{Z_P^2 Z_T^2 e^4}{4\pi\epsilon_0^2 A_P m_P} \cdot \frac{n_{at}}{V^2} \cdot (G_i \cdot L_i + H_i \cdot \log(X_i)), \quad \text{with :} \quad (2.15)$$

$$\begin{aligned}
X_i &= V/V_i \\
L_i &= \log(\lambda_{D_i}/b_i) \\
G_i &= \operatorname{erf}(X_i/\sqrt{2}) - \sqrt{2/\pi} \cdot X_i \cdot e^{-(X_i^2)/2} \\
H_i &= (-X_i^3 \cdot e^{-(X_i^2)/2})/(3\sqrt{2\pi}) + X_i^4/(X_i^4 + 12)
\end{aligned}$$

On the other hand $S_{p_{bound}}$, is develop by us in the context of a rapid and linear ion-ion collision in Born approximation, following the ideas of X. Garbet [3].

Bound electron stopping:

$$S_{p_{Bound}}(V, T, n_{at}) = \frac{Z_P^2 e^4}{4\pi\epsilon_0^2 m_e} \cdot \frac{n_{at}}{V^2} \cdot (Z_T - \bar{Z}_T) \cdot L_b, \quad \text{with :} \quad (2.16)$$

$$\begin{aligned}
L_b &= \left(\log\left(\frac{2m_e V^2}{I_b}\right) - \frac{4Ek_b}{2m_e V^2} \right), & \text{if } V > V_{int} \\
L_b &= \left(\frac{V^3 \cdot \alpha}{1 + G \cdot V^2} \right), & \text{if } V < V_{int}
\end{aligned}$$

$$\text{and } \alpha = 1.067 \frac{\sqrt{Ek_b}}{I_b^2}; \quad G = V_{int}^{-1} \cdot \left(\frac{V_{int}^3 \cdot \alpha}{\log(2V_{int}^2/I_b) - (2Ek_b/V_{int})} - 1 \right)$$

In the last three equations, e is the electron charge, m_e is the electron mass, m_P is the proton mass, ϵ_0 is the vacuum permitivity, Z_P is the charge of the projectiles of the beam, Z_T is the charge of the plasma element, \bar{Z}_T is the plasma average ionization or mean charge, n_{ef} is the free electron density, n_{at} is the atom density, V is the velocity of the projectiles of the beam, V_e is the thermal velocity of the free electrons, V_i is the thermal velocity of the ions (mass centers), λ_D is the Debye length and b is a impact parameter for a minimum collision distance (both for electrons and ions), I_b is the mean excitation energy of the bound electrons of the plasma ions, Ek_b is the average kinetic energy of bound electrons of the plasma and $V_{int} = \sqrt{3Ek_b + 1.5I_b}$. The magnitudes \bar{Z}_T , Ek_b and I_b are calculated using the collisional-radiative model, which is explained in the section 2.4 of this chapter.

At this point, it is important to highlight that in our stopping expression the parameters have an spatial dependence, so, when a beam is interacting within a plasma of length L , equation 2.8 can be written as:

$$\frac{dEk(x)}{dx} = -Sp (Ek(x); T(x), \rho(x), \bar{Z}_T(x)) \quad (2.17)$$

2.3 Heating of the Plasma

This section will cover the physical model used to simulate the heating of the plasma as the beam yield its energy in it. The equation that governs the change in the energy of the plasma per volume (\mathcal{E}) is given by:

$$\begin{aligned} \frac{\partial \mathcal{E}(x, t)}{\partial t} + \vec{V} \cdot \vec{\nabla} \mathcal{E}(x, t) = \\ = \frac{d\mathcal{E}_{cond}(x, t)}{dt} + \frac{d\mathcal{E}_{rad}(x, t)}{dt} + \frac{d\mathcal{E}_{dif}(x, t)}{dt} + \frac{d\mathcal{E}_{beam}(x, t)}{dt} + \frac{d\mathcal{E}_w(x, t)}{dt} \end{aligned} \quad (2.18)$$

Where is taken into account the heat conduction, the radiation energy, the diffusion, the convection processes, the mechanical work and, in this case, the energy transferred by interaction process with a beam.

In our heating plasma model, the ion beam duration Δt_{beam} is considered short enough in comparative with the characteristic hydrodynamic time of each one of the plasma processes commented above: $\Delta t_{beam} \ll \Delta t_H$. Therefore, it can be assumed that during the interaction time between the plasma and the beam (or heating time), there is no energy change by conduction, diffusion or radiation in the volume. Moreover, we assume an isochoric heating where the plasma is in rest, so there is no mechanical work and convection. Under this conditions, equation 2.18 can be reduced to:

$$\frac{d\mathcal{E}(x, t)}{dt} = \frac{d\mathcal{E}_{beam}(x, t)}{dt}; \quad \text{with } (0 < t < \Delta t_{beam}) \text{ and } (0 < x < L) \quad (2.19)$$

Now, admitting an ideal state equation, the energy per volume of the plasma is given by:

$$\mathcal{E}(x, t) = \rho(x, t) C_V(x, t) T(x, t) \quad (2.20)$$

Where the matter density ρ is consider in isochoric conditions during the beam-plasma interaction so it has only spatial dependence $\rho(x)$, the temperature represents a field $T(x, t)$ and the heat capacity at constant volume $C_V(\rho(x, t), T(x, t)) = C_V$ is consider fixed [8] during the interaction time as the process is isochoric.

So, equation 2.19 is written as:

$$\rho(x) C_V \frac{dT(x, t)}{dt} = \frac{d\mathcal{E}_{beam}(x, t)}{dt} \quad (2.21)$$

On the other hand, the beam interaction term is defined as a flux of particles per time $db(t)/dt$, multiplied by the energy variation of the plasma per ion and path length:

$$\frac{d\mathcal{E}_{beam}(x, t)}{dt} = \frac{db(t)}{dt} \frac{d\mathcal{E}_{ion}(x, t)}{dx} \quad (2.22)$$

Aiming to evaluate the energy deposited by the ion beam in the plasma, it is considered that the beam interaction time (or heating time) Δt_{beam} must be larger or equal to the projectile deceleration time or flight time, $\Delta t_{flight} \leq \Delta t_{beam}$, at the path length in the plasma.

Thus, there are two time scales, Δt_{flight} and Δt_{beam} that allow to determine how the projectile yields energy in the plasma:

$$\Delta t_{flight} \leq \Delta t_{beam} \ll \Delta t_H \quad (2.23)$$

When $t \in \Delta t_{beam}$, we can calculate the energy variation of the plasma per ion and length considering the stopping power as a field. This field $Sp(x, t)$, is obtained as the energy loss of the projectile through the plasma for each instant of time.

$$\frac{d\mathcal{E}_{ion}(x, t)}{dx} = Sp(x, t), \quad \text{where } t \in \Delta t_{beam} \quad (2.24)$$

These stopping power values are given by expressions 2.14, 2.15 and 2.16. Finally, expression 2.21 can be written in terms of equation 2.22, using the change of 2.24:

$$\frac{dT(x, t)}{dt} = \frac{1}{\rho(x) C_V} \frac{db(t)}{dt} Sp(x, t) \quad (2.25)$$

Evaluated in a plasma of length $0 < x < L$, during the beam interaction heating time $0 < t < \Delta t_{beam}$.

Moreover, as it has been seen in section 2.2.4, Sp_{free} , Sp_{ion} and Sp_{bound} have a dependence with the velocity of the projectile, the temperature, the density and the mean charge of the plasma. This section shows that the temperature changes when a flux of projectiles enter the plasma, thus stopping power equation 2.17 will have a time dependence.

$$\frac{dEk(x(t))}{dx} = -Sp (Ek(x), T(x, t), \rho(x), \bar{Z}_T(x, t)) \quad (2.26)$$

Equation 2.25 can be written taken into account all the dependences of the stopping power:

$$\frac{dT(x, t)}{dt} = \frac{1}{\rho(x) C_V} \frac{db(t)}{dt} Sp (Ek(x), T(x, t), \rho(x), \bar{Z}_T(x, t)) \quad (2.27)$$

2.4 Atomic Kinetic Equations Plasma

As have been explained in the previous section 2.2.4, certain parameters needed to calculate the stopping power are externally calculated. For example, the populations per volume of the plasma components $P_{q,i}$ corresponding to the q^{th} state charge (neutral, once ionized...) and the i^{th} atomic state (ground state, first excited state...). This involves the calculation of the atomic structure of each quantum level and the cross sections of the atomic processes in the plasma by solving Dirac equations. Finally it is necessary, to built and solve the collisional-radiative equations to obtain the populations of the plasma.

The physical model that characterizes the plasma and calculates the populations will be explained in this section and the computational implementation of this model (MIXKIP code) is explained in the next chapter 3.

Collisional-Radiative model

In a plasma, its components are constantly suffering processes that will define its microscopic state of the plasma. To describe this processes of the plasma, each cross section and rate is necessary: the cross section ($\sigma_{i \rightarrow f}(V)$) gives the probability of a process between an initial and final states and the rates ($r_{i \rightarrow f}$) give the corresponding number of reactions per volume and time.

Once the rates of all processes are determined, the system of equation that gives the temporal variation of the population of any ion or atom, for each q ($0, \dots, Z$) and i level, is:

$$\frac{dP_{q,i}(\vec{r}, t)}{dt} = \sum_{q',j} P_{q',j}(\vec{r}, t) \mathbb{R}_{(q',j) \rightarrow (q,i)}^+ - \sum_{q',j} P_{q,i}(\vec{r}, t) \mathbb{R}_{(q,i) \rightarrow (q',j)}^- \quad (2.28)$$

Where \mathbb{R}^+ is the matrix with all the rates of processes that increase the population of $P_{i,q}$, and \mathbb{R}^- , is the matrix with all the rates that depopulate $P_{i,q}$. Moreover, this system of equations is calculated, for a given free electron density n_{ef} and temperature T and under the restrictions of particle number (n_{at}) conservation, given by:

$$\sum_{q,i} P_{q,i} = n_{at} \quad (2.29)$$

And considering a neutral plasma:

$$\sum_{q,i} qP_{q,i} = \frac{n_{ef}}{n_{at}} \quad (2.30)$$

The most significant processes that account populating and depopulating mechanisms are:

Direct process	Inverse process
Spontaneous decay	Absortion
Collisional ionization	3-Body recombination
Collisional excitation	Collisional deexcitation
Photo-ionization	Radiative recombination
Self-ionization	Electronic capture
Bremsstrahlung	Inverse Bremsstrahlung

Equation 2.28 describes a general thermodynamic state of the internal structure of the ions of the plasma. In a plasma in which the rate of the ionizations is larger than the rate of recombinations, is called *ionizing plasma*, on the other hand, in a plasma where the rate of recombinations is larger than the rate of ionizations, it is called a *recombining plasma*. Additionally, a *steady state* is attained when both rates are equal, then the variation of the populations is null and the atomic level populations are time independent. All this regimes are described as Non Equilibrium Thermodynamical Regimens (NLTE).

Among the various steady states of a plasma, the Local Thermodynamical Equilibrium (LTE) state is the closest to the complete Thermodynamical Equilibrium (TE). In TE conditions the rates of each process, of the three types of particles (ions, electrons and photons), equals exactly the rate of the inverse.

Then, LTE occurs in plasmas whose dimensions are significantly smaller than the mean free path of the photons emitted from the plasma, but are much longer than the collisional length of the electron and the ions. In LTE, the electrons and the ions are in equilibrium among themselves, whereas the photons are not. So, the electrons and ions has its corresponding temperatures [9].

In this work the NLTE situations considered correspond to a system were the electrons are in equilibrium, but the internal structure of the ions is in non-equilibrium. Then, we assume that the ions have the same temperature as the electrons.

Additionally, in this section we show how the values of the populations P_{ij} are used to calculate the average ionization \bar{Z}_T , the average excitation I_b and the average kinetic energies of the bound electrons E_{kb} . This parameters are used to calculate the bound electron stopping power of section 2.2.4:

$$\bar{Z}_T = \sum_{qi} qP_{qi} \quad (2.31)$$

$$E_{kb} = \frac{1}{Z_T - \bar{Z}_T} \sum_{q,i} P_{qi} N_q K_{qi}; \quad \left(K_{qi} = \frac{1}{N_q} \sum_k w_{qik} K_{qik} \right) \quad (2.32)$$

$$I_b = \prod_{qi} I_{qi}^{\frac{P_{qi} N_q}{Z_T - \bar{Z}_T}}; \quad \left(I_{qi} = \prod_k I_{qik}^{\frac{w_{qik}}{N_q}}; \quad I_{qik} = \sqrt{\frac{2K_{qik}}{\langle r^2 \rangle_{qik}}} \right) \quad (2.33)$$

Where N_q is the number of bound electrons of an ion of charge q ; w_{qik} denotes the number of electrons in the k monoelectronic state of the ion in the q, i state; $\langle r \rangle_{qik}$ is the mean radius and, finally, K_{qik} and I_{qik} are the monoelectronic kinetic and the mean excitation energies.

When a beam interacts with the plasma, the collisional-radiative must be expanded. Then, the rate equations corresponding to the atomic level populations of the beam are included. Moreover, new ion beam-ion plasma interaction processes must be taken into account, in particular the ion-ion collision and charge transfer.

This two processes are not included in MIXKIP yet, however have been studied in the Appendix, because its computational implementation is considered as a future work line.

2.5 Summary of the Physical Model

The equations that our numerical model has to solve to simulate the plasma-beam interaction are 2.26 and 2.27:

$$\frac{dEk(x)}{dx} = -Sp (Ek(x); T(x, t), \rho(x), \bar{Z}_T(x, t))$$

$$\frac{dT(x, t)}{dt} = \frac{1}{\rho(x) C_V} \frac{db(t)}{dt} Sp (Ek(x); T(x, t), \rho(x), \bar{Z}_T(x, t))$$

However, for the experiments that we will study the plasma has constant density and mean charge, so the previous expressions can be reduced to:

$$\frac{dEk(x)}{dx} = -Sp (Ek(x), T(x, t)) \quad (2.34)$$

$$\frac{dT(x, t)}{dt} = \frac{1}{\rho C_V} \frac{db(t)}{dt} Sp (Ek(x), T(x, t)) \quad (2.35)$$

Where $0 < x < L$ and $0 < t < \Delta t_{beam}$

Chapter 3

Numerical and Computational Models

Once the physical model of the beam-plasma interaction process has been explained, we can tackle the numerical approaches to the problem and the computational implementation in the STOPBIN code. Moreover, the structure of MIXKIP code and the method to solve the collisional-radiative equations are explained, which provides input parameters to the STOPBIN code.

3.1 Numerical Approaches to the problem

In this section we show the numerical approaches based in finite differences, used to solve the differential equations that define the problem. A brief description of the Euler method and Runge-Kutta method are presented, where the first one is used to solve equation 2.35 and the second one to solve equation 2.34. Then, there is an explanation of the error is estimated and how an adaptive mesh is implemented to solve the equation 2.34.

3.1.1 Euler method

The Euler method is a first order numerical procedure for solving ordinary differential equations [10]. Given a differential equation and its initial values:

$$\frac{dy(x)}{dx} = f(x, y), \quad y(x_0) = y_0 \quad (3.1)$$

the Euler method, in the forward difference form, computes the solution of y in the mesh $x_1 \dots x_N$, as:

$$\hat{y}_{n+1} = \hat{y}_n + hf(x_n, y_n) \quad (3.2)$$

Where $h = x_{n+1} - x_n = \Delta x_n$ is the step for each iteration and N is the total number of nodes used in the discretization. In the Euler method the local error is proportional to the square of the step size, and the overall error is proportional to the step size.

3.1.2 Runge Kutta method

The Runge Kutta method of n^{th} order gives approximate solutions to ordinary differential equations [11]. Given a differential equation and its initial conditions:

$$\frac{dy(x)}{dx} = f(x, y) \quad (3.3)$$

this method, in the 4^{th} order, computes the solution of y in the mesh $x_1 \dots x_N$, as:

$$\hat{y}_{n+1} = \hat{y}_n + \frac{h}{6} \sum_{i=1}^4 k_i \quad (3.4)$$

$$\begin{aligned} k_1 &= f(x_i, \hat{y}_i) \\ k_2 &= f\left(x_i + \frac{1}{2}h, \hat{y}_i + \frac{1}{2}k_1h\right) \\ k_3 &= f\left(x_i + \frac{1}{2}h, \hat{y}_i + \frac{1}{2}k_2h\right) \\ k_4 &= f(x_i + h, \hat{y}_i + k_3h) \end{aligned}$$

Where $h = x_{n+1} - x_n = \Delta x_n$ is the step for each iteration and k_i are the halfway approximation terms, evaluated in f locally.

In the Runge-Kutta method k_i represent the estimated slopes using the midpoints of the interval. Thereby, k_1 is the slope at the beginning of the interval, k_2 is the slope at the midpoint of the interval, using k_1 to determine the value of y at the point $x_n + h/2$ with the Euler method. Then, k_3 is again the slope of the midpoint, but now using k_2 to determine the value of y ; k_4 is the slope at the end of the interval, with the value of y determined by k_3 . Averaging the four slopes, greater weight is assigned to the slopes at the midpoint:

$$slope = \frac{k_1 + 2k_2 + 2k_3 + k_4}{6}$$

As this is a fourth order method, its associated error per step is of the order of $O(h^5)$, the total error is of the order of $O(h^4)$ and so, the order of convergence of the method is $O(h^4)$.

3.1.3 Error Estimation

The absolute error (e) of both Euler and Runge-Kutta methods depends on the size of the step and is given by:

$$e_i(h) = |\hat{y}_i - y(x_i)| \quad (3.5)$$

As the analytical solution (y) of our differential equations is unknown, we estimate the error of the approximated solution obtained with step h ($\hat{y}[h]$), comparing it with those obtained using a refined mesh. In particular, in our analysis of the error estimation, the refined mesh is built with a half sized step ($h/2$). The relative error

is calculated as the difference between the solution points shared in both mesh.

$$error_i = \frac{|\hat{y}_i[h] - \hat{y}_i[h/2]|}{\hat{y}_i[h/2]} \quad (3.6)$$

3.1.4 Adaptive Mesh

Solving a differential equation with an adaptive mesh provides an approximated solution with a non uniform mesh, which adapts dynamically the step size [12], evaluating the error.

In our model, given an initial step size h , this method calculates $\hat{y}_i[h]$ and $\hat{y}_i[h/2]$. If the relative error given by equation 3.6 is lower than a tolerance threshold (τ), the method keeps the solution $\hat{y}_i[h/2]$ and proceeds to calculate the solution in the next node ($\hat{y}_{i+1}[h]$). If the tolerance threshold condition is not fulfill, the step is divided again and this procedure is repeated until the tolerance condition is reached.

Using this method, the solution has a refined mesh in the regions where is needed and a more rough mesh in the regions where the error among the solutions is lower. This procedure can be synthesized as:

$$error_i = \frac{|\hat{y}_i[h] - \hat{y}_i[h/2]|}{\hat{y}_i[h/2]} \quad (3.7)$$

if $error_i > \tau$: evaluation with $h'_i = \frac{h_i}{2}$

if $error_i < \tau$: next node, $i = i + 1$

3.2 Discretization of the Physical Model

The differential equations of section 2.5 are solved using numerical methods, so it is necessary to present a discrete form of this expressions.

3.2.1 Discretization of the Plasma and the Energy Loss

The stopping power governs the variation of the kinetic energy of the beam per length unit. It depends on the velocity of the projectile, in each position and instant, and the temperature of the plasma, as it was shown in equation 2.34, written as:

$$\frac{dEk(x)}{dx} = -Sp(Ek(x); T) \quad (3.8)$$

with:

$$Ek(x_0) = Ek_0 \quad \text{and} \quad 0 < x < L$$

This monodimensional problem is discretized in a set of N_x nodes, where the step is $\Delta x = L/N_x$ and the mesh is given $x_n = n \cdot \Delta x$. Then, the solution using the Euler method is:

$$\frac{Ek_{n+1} - Ek_n}{\Delta x} = -Sp_n$$

or:

$$Ek_{n+1} = Ek_n - Sp_n \cdot \Delta x \quad (3.9)$$

Taken into account that the stopping power is defined positive, the stopping power reduces the kinetic energy (Ek) of the ion beam in each n^{th} point of the mesh. This equation is solved with an adaptive mesh, as the results show in section 4.1.2.

Another magnitude to define is the *range*, which is the maximum depth reached by the projectile in the plasma. It is calculated as the point where the projectile has lost all its energy:

$$range = x_n, \quad \text{where} \quad Ek_n = 0 \quad (3.10)$$

Equation 3.9 works when the beam is made up of one single projectile. So, a more convenient way to express the interaction between the beam and the plasma requires the presence of an index that indicates the instant of time, in which the associated bin suffers the energy loss in a given plasma state. Following this ideas, equation 3.9 is expressed for the m^{th} bin that enters the n^{th} node of the plasma as:

$$Ek_{n+1,m} = Ek_{n,m} - Sp_{n,m} \cdot \Delta x \quad (3.11)$$

Although, this equation is written in the Euler method formalism it will solved using a Runge-Kutta method. Also, it is important to highlight the dependence of the stopping power with the kinetic energy of the projectile and the temperature of the plasma:

$$Sp_{n,m} = Sp(Ek_{n,m}, T_{n,m})$$

The Figure 3.1 shows how the m^{th} bin enters the plasma.

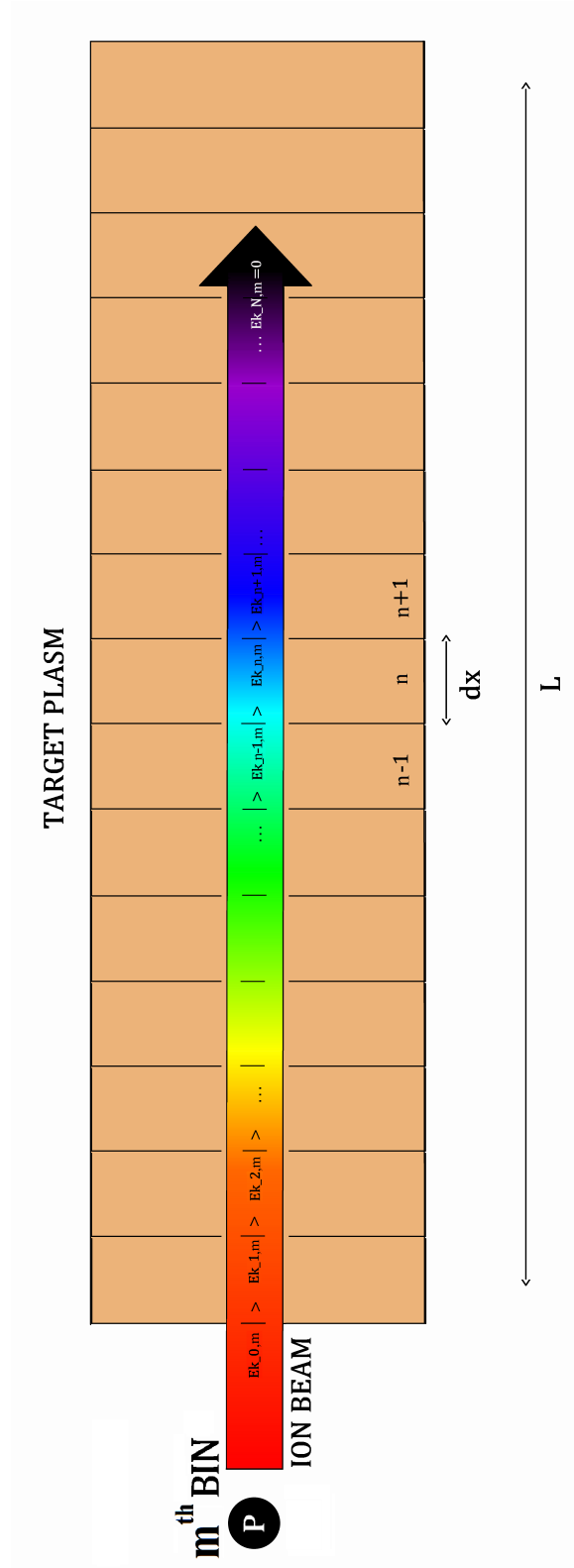


Figure 3.1: Discrete model of the plasma with a projectile beam.

3.2.2 Discretization of the Temperature Equation

The stopping power governs the heating of the plasma and so, the value of the temperature, as shown in equation 2.35:

$$\frac{dT(x, t)}{dt} = \frac{1}{\rho C_V} \frac{db(t)}{dt} Sp(x, t) \quad (3.12)$$

In this equation, $db(t)/dt$ represents the flux of particles per time that enter the plasma and in this work it is considered constant B . Moreover, for the n^{th} node the expression 2.35 is written as:

$$\frac{dT(x_n, t)}{dt} = \frac{B}{\rho C_V} Sp(x_n, t) \quad (3.13)$$

Then, the solution applying the Euler method is:

$$\frac{T_{n,m+1} - T_{n,m}}{\Delta t} = \frac{B}{\rho C_V} Sp_{n,m} T_{n,m+1} = T_{n,m} + \frac{B}{\rho C_V} Sp_{n,m} \Delta t$$

Or:

$$T_{n,m+1} = T_{n,m} + \frac{B}{\rho C_V} Sp_{n,m} \Delta t \quad (3.14)$$

Now, taken into account the following relations:

$$\frac{db(t)}{dt} = B \rightarrow db = B dt \rightarrow \Delta b = B \Delta t;$$

Then, equation 3.14 is now written:

$$T_{n,m+1} = T_{n,m} + \frac{1}{\rho C_V} Sp_{n,m} \Delta b \quad (3.15)$$

Where Δb is a partition of the beam flux, which is called *bin*. If the the flux b is discretized in N_b nodes, then the ion beam flux is considered split into N_b bins that are successively passed through the plasma. Each bin is compound as group particles that move in the plasma together, at the same time. This change (time \rightarrow bin) is very useful, because allows to tackle the problem without treating explicitly the time and the particle flux [8]. Therefore, equation 3.15 shows the change in the plasma temperature due to m^{th} bin in the n^{th} spatial node.

Moreover, the value of the beam discretization Δb is usually described as:

$$\Delta b = \frac{Q}{N_b Ek_0} \quad (3.16)$$

Where Q is the energy flux of the beam and Ek_0 is the initial kinetic energy of the projectiles, so Δb units are number of projectiles (n_P) in a bin per surface unit.

3.2.3 Summary of the Discrete Problem

Here is presented a discretized form to solve the differential equation 2.34 which depends on the results of another differential equation, 2.35, both with defined initial and boundary conditions.

$$\bullet Ek_{n+1,m} = Ek_{n,m} - Sp_{n,m}\Delta x;$$

$$\bullet T_{n,m+1} = T_{n,m} + Sp_{n,m}\frac{1}{\rho C_V}\Delta b;$$

$$\text{With: } N_x\Delta x = L \text{ and } N_b\Delta b = Q/Ek_0$$

Initial conditions: $Ek(x=0) = Ek_0$ and $T(x, t=0) = T_0$.

Boundary conditions: $x \in [0, L]$ and $b \in [0, Q/Ek_0]$.

3.3 MIXKIP Code

This section is devoted to the explanation of MIXKIP code, as well as to comment some computational aspects related to the resolution of the equations.

MIXKIP [13] is a Fortran computational package that calculates the atomic structure and atomic kinetic of the ions in the plasma by solving the set of rate equations in collisional-radiative formalism. This computational package combines a set of theoretical and numerical approximations which yield a substantial saving in computing running time, but are still reliable enough compared with more elaborated codes and experimental data.

To tackle the problem explained in the previous section, MIXKIP code solves the microscopic problem in stationary situation for a cylindrical, spherical or a planar geometries, for different chemical elements (H,..., He,..., C., Al., Fe,..., Xe,..., Au,...), under a large set of macroscopic conditions of density and temperature. Also, it has application in plasmas in thermodynamic local equilibrium and outside of it. MIXKIP code can solve the rate equations or Saha-Boltzmann equations to calculate the ion populations of the plasma for different conditions. However, Saha-Boltzmann equations are only valid when the plasma is in the LTE regimen, and in this situations, rate equations and Saha equations provide the same results. In this analysis, the calculations to determine the ion populations obtained from rate equations are labeled as NLTE while those obtained from Saha-Boltzmann equations, as LTE.

MIXKIP will obtain the values of the ion populations of the plasma, the mean ionization, average charge and average energy. MIXKIP needs an input with the selected atomic configurations of the ions, the geometry of the problem, its temperature and matter density or free electron density. In this work it is assumed that the plasma is optically thin, i.e, electromagnetic radiation or photons are not reabsorbed by matter, so the set of rate equations do not depend on the geometry and are uncoupled.

The MIXKIP code is composed by two main modules: atomic structure module and atomic kinetic (collisional-radiative) module. Once the atomic structure data and the atomic level populations have been calculated, MIXKIP code launches the radiative properties module, in which are obtained the spectroscopy magnitudes that characterize the plasma. Below are explained the two main modules of MIXKIP and it is shown a flowchart of the code in figure 3.2.

Atomic Structure module

MIXKIP has a built-in model to obtain all atomic data required to characterize the internal structure of the ions, to calculate the cross section of the collisional and radiative processes and for the atomic kinetic calculations. For each single-electron level of each atomic configuration defined in the input, the Dirac equation is solved by a fourth order Runge-Kutta method in a linear or exponential radial mesh. There are many atomic equations, the order of configurations considered (around $10^3 - 10^5$). They are coupled with atomic kinetic equations by means of the average ionization of the plasma, and therefore, they must be solved iteratively. At high temperature and low density, the effective potential tends to the isolated one, and the atomic

and atomic kinetic equations became uncoupled.

On the other hand, although the number of atomic levels for a given isolated ion is infinite, due to the coulomb interaction between the bound electrons and the surrounding plasma, this number should be finite to obtain a satisfactory simulation of their radiative properties. Therefore, it is necessary to make a previous selection of the atomic configurations and levels. However, there is not a priori criterion to determine which configurations should be included in the model. In general, the kind of configurations to include depends on the plasma conditions, the presence of external radiation fields or the interaction with particle beams. The experience achieved, based on the large number of cases studied during the development of the computational package, took us to choose a proper complete enough set of configurations which allow us to obtain reasonable average ionization and ion abundances or populations. This set of configuration must be wide enough to obtain reasonable radiative properties of the plasma. In this case, the criterion employed was based on a rule of thumb, in which the configurations included for each ion are those with energies up to twice the ionization energy of the ground configuration.

Population Kinetics module

This module gives the population or abundance distribution, by solving a rate equation system, which describes the population density of atomic configurations or states. It follows the standard non equilibrium modeling approach, based on the consideration of the microscopic collisional-radiative processes between different atomic configurations (or levels).

Given a T temperature and a n_{ef} free electron density, the MIXKIP code solves the collisional radiative model to obtain the populations of the plasma P_{ij} . When the electron density is take into account as an input parameter, the set of the rate or atomic kinetic equations constitutes a linear system of M equations, where M is the total number of atomic states included in the atomic module. Also, the matter density ρ can be used as an input with the temperature, and in this case, the equation system is non-linear and it is solved an iterative procedure.

The collisional-radiative atomic processes in the plasma only connects levels that belong either to same charge state or to adjacent ones, which leads to sparse linear system. Thus, in order to keep memory requirements to a minimum, MIXKIP uses sparse techniques to store and operate on only non zero matrix elements. Additionally, in an atomic kinetic problem the number of level can easily reach the order of $10^3 - 10^5$; hence, the code uses an iterative method to perform the matrix inversion, because it typically computes the solution faster than direct (standard) method. In the time dependent problems, the forward pass Euler method is used to discretized the first order temporal derivative.

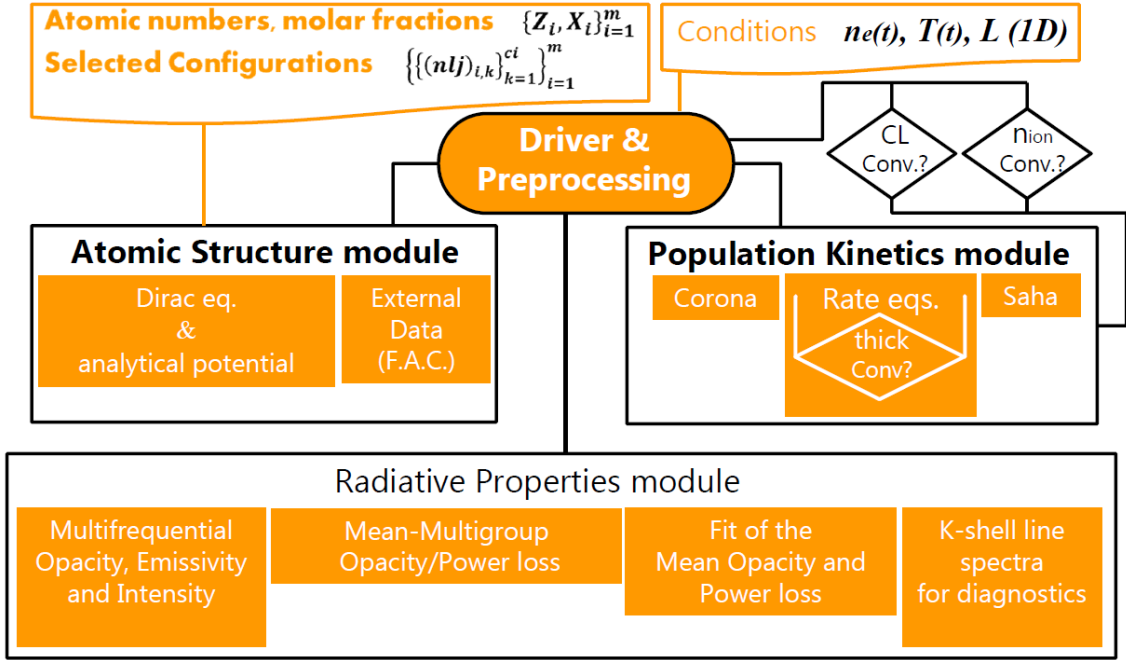


Figure 3.2: Flowchart of MIXKIP code.

3.4 Computational Implementation: STOPBIN

The interaction between an ion beam and a plasma is settled in section 2.5 as a pair of differential equations, and then discretized in the section 3.2.3. To solve this problem a set of codes were developed and brought together in the program called STOPBIN. In the code are implemented the stopping power expressions from section 2.2.4. This expressions are solved with the set of input values that STOPBIN requires to simulate the interaction and obtain the values of the temperature and the kinetic energy.

The inputs of STOPBIN include the following parameters:

- Atomic beam composition (A_P, Z_P).
- Range of initial kinetics energies of the beam for every 'm' projectile (Ek_0).
- Number of bins in which is divided the beam (N_b).
- Flux of the energy per particle that enters the plasma (ΔQ)
- Atomic plasma composition (A_P, Z_P).
- Initial temperatures of the plasma for all 'n' ($T_{n,0}$).
- Free electron density (n_{ef}) or matter density (ρ).
- Average ionization (\bar{Z}_T).
- Average kinetic energy of the bound electrons (Ek_b).
- Average excitation energy of the bound electrons (I_b).
- Heat capacity of the plasma (C_V).
- Length if the plasma (L).
- Points of the mesh that discretize the plasma (N_x).

Solving Procedure

STOPBIN solves pair of differential equations given in section 3.2.3. As both equations are coupled by the dependences of the stopping power function, the procedure alternates solving the kinetic energy equation and the temperature equation.

First, the kinetic energy equation is solved using a Runge-Kutta 4th algorithm and the values of the stopping power and the kinetic energy are obtained in all n points, in a certain m^{th} .

Then, this solutions will be used to solve temperature equation with an Euler method and calculate the new values of the temperature $(m+1)^{th}$ in all the n points.

This new temperature will be introduce in the first equation to calculate the kinetic energy and the stopping power in all the n points for the next m^{th} bin. Later, this solutions will be introduced in the temperature equation again.

This procedure will continue until all the bins have dig in the plasma i.e, all the kinetic energy, stopping and temperature values have been obtained for every bin and position node. In figure 3.3 there is graphic example of this procedure. Moreover, the following pseudocode and the example below will clarify the calculation process.

Pseudocode

STOPBIN MAIN function launches the rest of functions:

1. Data Set with Physical Constants, that will be used in the rest of the functions.
2. Input values for both plasma and beam parameters
3. Numerical procedure:

```

for m=(1:N_b)

    for n=(1:N_x)
        RK4: Ek(n+1,m)=Ek(n,m)-Sp(Ek(n,m),T(n,m))*dx
    end

    Euler: T(n,m+1)=T(n,m)+Sp(Ek(n,m),T(n,m))/(rho Cv)*db
    (Solved vectorizing for all 'n' between 0 and N_x)

end

```

4. Output values of the kinetic energy (Ek), the stopping power (Sp) and the temperature (T).

It is important to highlight that the temperature calculation does not need a solution procedure in the lengthwise dimension ($n \rightarrow n + 1$), because the solution in each spatial node does not depend directly of its neighbors and exploiting the vectorizing capabilities of Matlab, it is not necessary to use any loop.

The kinetic energy equation is solved using a Runge-Kutta method because its solutions show sharper slope changes, so it will require a more precise solution. The temperature equation uses a Euler method instead of a Runge-Kutta because its results are smoother and computational time is saved.

Below is shown an example with the calculation of the results and its related figure 3.3:

Initial known values: $Ek_{0,0} \dots Ek_{0,Nb}; \quad T_{0,0} \dots T_{Nx,0}$

First:

$Ek_{n+1,0} = Ek_{n,0} - Sp(Ek_{n,0}, T_{n,0})$ is solved in all the spatial nodes $n \in [0, Nx]$

Second:

$T_{0,1} = T_{0,0} + Sp(Ek_{0,0}, T_{0,0})$

$T_{1,1} = T_{1,0} + Sp(Ek_{1,0}, T_{1,0})$

...

$T_{Nx,1} = T_{Nx,0} + Sp(Ek_{Nx,0}, T_{Nx,0})$ independent equations, parallel procedure

Third:

$Ek_{n+1,1} = Ek_{n,1} - Sp(Ek_{n,1}, T_{n,1})$ is solved in all the spatial nodes $n \in [0, Nx]$

Fourth:

$T_{0,2} = T_{0,1} + Sp(Ek_{0,1}, T_{0,1})$

$T_{1,2} = T_{1,1} + Sp(Ek_{1,1}, T_{1,1})$

...

$T_{Nx,2} = T_{Nx,1} + Sp(Ek_{Nx,1}, T_{Nx,1})$ independent equations, parallel procedure

Fifth:

$Ek_{n+1,2} = Ek_{n,2} - Sp(Ek_{n,2}, T_{n,2})$ is solved in all the spatial nodes $n \in [0, Nx]$

...

Nb-th:

$Ek_{n+1,Nb} = Ek_{n,Nb} - Sp(Ek_{n,Nb}, T_{n,Nb})$ is solved in all the spatial nodes $n \in [0, Nx]$

Nx-th:

$T_{0,Nb} = T_{0,Nb-1} + Sp(Ek_{0,Nb}, T_{0,Nb-1})$

$T_{1,Nb} = T_{1,Nb-1} + Sp(Ek_{1,Nb}, T_{1,Nb-1})$

...

$T_{Nx,Nb} = T_{Nx,Nb-1} + Sp(Ek_{Nx,Nb-1}, T_{Nx,Nb-1})$ independent equations, parallel procedure

3.4.1 Additional Features

Furthermore, taken advantage vectorizing capabilities of Matlab, the code obtains simultaneously the solutions of the kinetic energy, the stopping power and the temperature, for a range of different initial kinetic energies ($Ek_0 = [Ek'_0, Ek''_0, Ek'''_0 \dots]$), without using additional loops. Thereby, the outputs of STOPBIN will consist in three tensors with the values of the kinetic energy of the beam, its stopping power

and the temperature of the plasma, for every spatial point, every initial kinetic energy of the beam and every bin that goes through the plasma. Figure 3.4 illustrates properly the storage procedure of the solutions as they are calculated.

Also, the range of each bin is calculated searching in the kinetic energy tensor the position of the first value where the bin has lost all its kinetic energy. Some Matlab functions have been exploited for quickly calculating the range values ($x(Ek = 0)$). In order to do this an equality condition is applied on the E matrix so that if the element is null, it will return a 0 and if it is not null, it will return 1. As the kinetic energy solutions will be positive until the bin has stopped, all the zeros and ones are arranged consecutively. Adding all the ones it is obtained the last position of each column of the matrix E that is different from 0. This value multiplied by the distance of the step gives the vector with the ranges that are obtain for each initial energy different from $E(0)$ and each m bin: $range = sum(Ek = 0) * dx$.

Finally, the error in the kinetic energy is calculated as the difference between its solution values for a mesh with step Δx and the following mesh with step $\Delta x/2$, in the points shared by both mesh. Similarly, the error in the temperature is calculated as the difference in the beam discretization between the points shared by a mesh with Δb and a mesh with $\Delta b/2$. Both expressions are presented below:

$$\frac{|Ek_{n,m}[\Delta x] - Ek_{n,m}[\Delta x/2]|}{Ek_{n,m}[\Delta x/2]} < \tau_{Ek} \tag{3.17}$$

$$\frac{|T_{n,m}[\Delta b] - T_{n,m}[\Delta b/2]|}{T_{n,m}[\Delta b/2]} < \tau_T$$

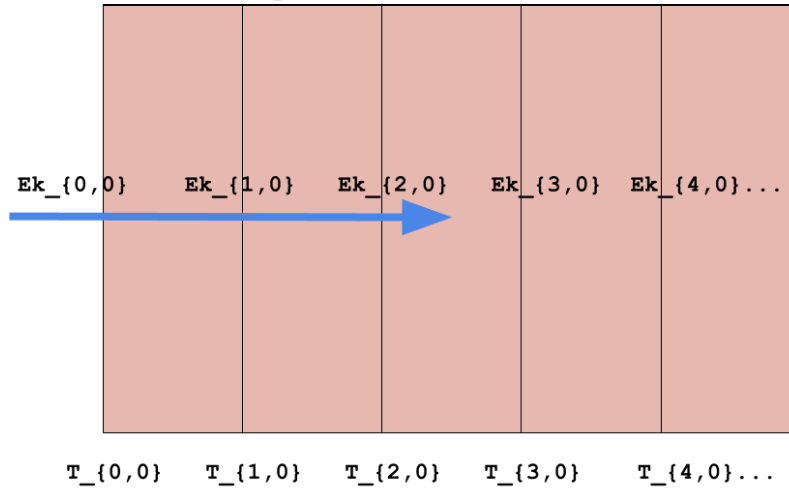
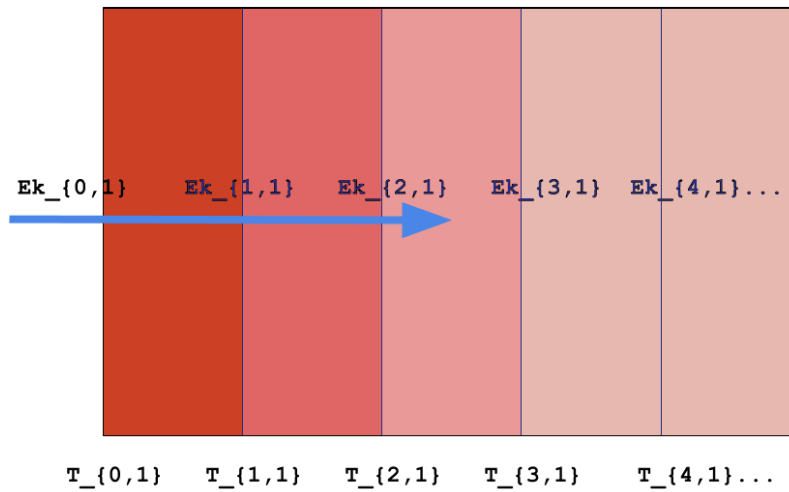
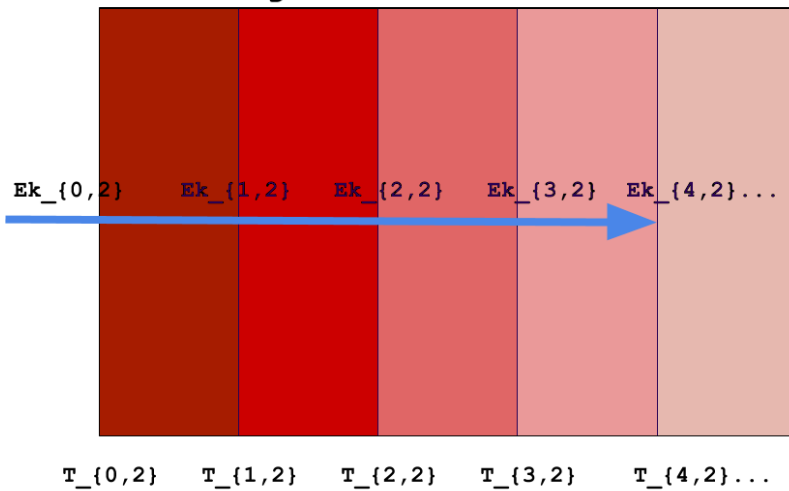
First Projectile**Second Projectile****Third Projectile**

Figure 3.3: Example of the STOPBIN solving procedure.

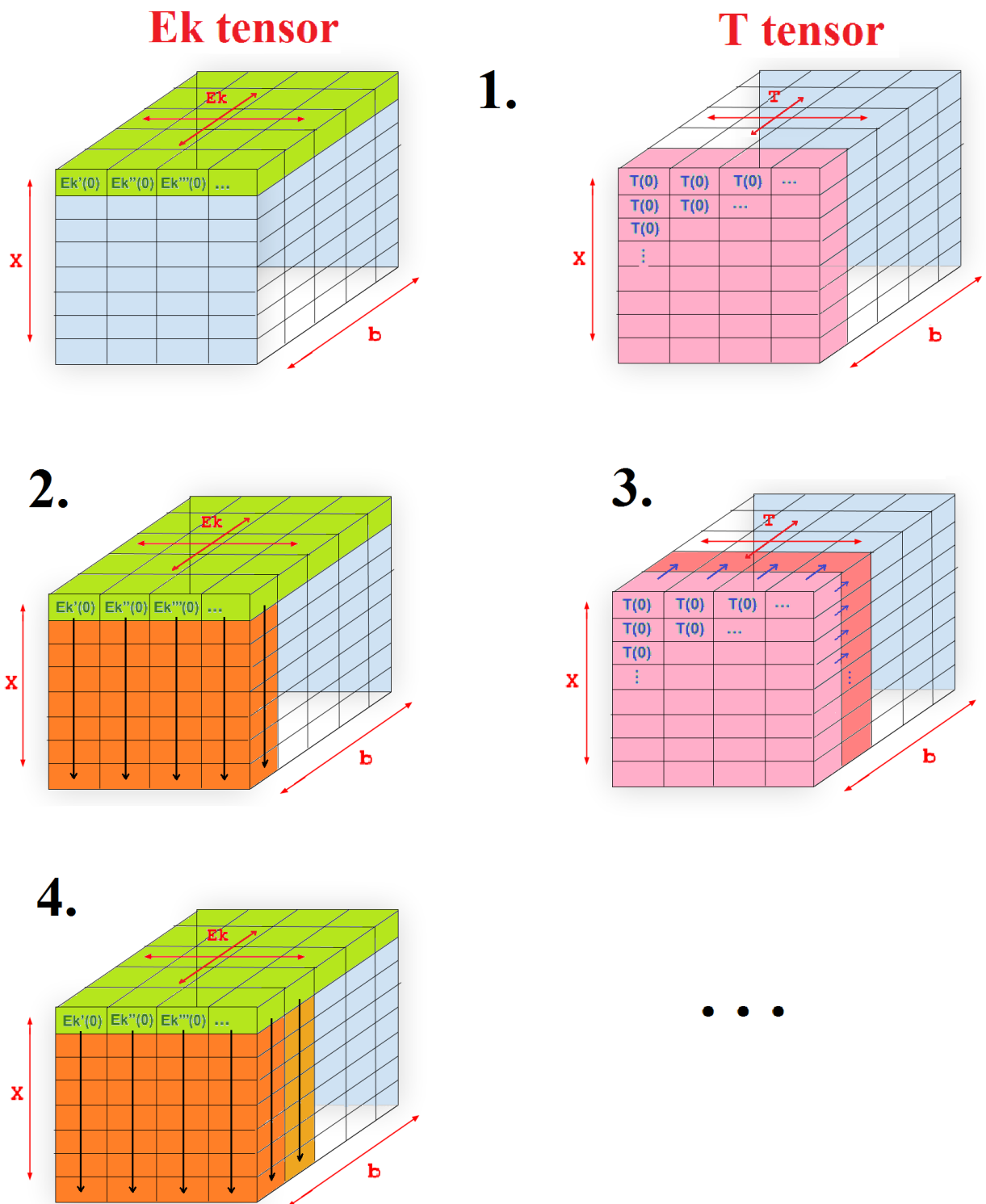


Figure 3.4: Processing and storage of the solutions in STOPBIN.

Chapter 4

Simulation and Results

Once the physical and numerical models have been implemented in the computational code STOPBIN, this chapter is organized as it follows: first, the numerical approach implemented in the code is internally tested; then, we check the validity of our model with external results; finally, we will present our own research of the behavior of a beam-plasma interaction, for different conditions.

4.1 Simulation Test

First, it is necessary to perform an internal test to acknowledge the limitations of our model and its error.

4.1.1 Numerical Model Test

In sections 3.1.3 and 3.4, it is explained that the mesh can be refined until the error in the kinetic energy and the temperature is lower than a threshold tolerance. The mesh is defined with the spatial discretization and the beam discretization (bins), if the error calculated between two different mesh is higher than the tolerance threshold settled for the experiment, the mesh will be refined.

In figure 4.1 it is shown the mean relative error of the kinetic energy and the temperature as a function of the number of nodes, both spatial and beam discretizations. Each error value is calculated as the difference between the actual mesh and the previous one, following expression 3.17. The relative error decreases when the mesh duplicate its nodes N_x and N_b . Also, the table 4.1 includes the computational times required using each number of nodes.

Moreover, it is observed that the kinetic energy error is always higher than the temperature error, although both are of the same magnitude order. This justifies choosing a Runge-Kutta method to solve the kinetic energy equation, since with an Euler method the expected error would be even greater. This behavior is understood taken into account that the kinetic energy have steeper slope changes than the temperature ones, as will be shown in this chapter.

In this work it is consider a proper tolerance threshold $\tau_{Ek} = \tau_T \sim 0.004$, i.e, 0.4%. Therefore, following the results of figure 4.1, the number of nodes to use in all experiments will be $N_x \geq 1000$ and $N_b \geq 1000$ and thus, the error of the simulations

is approximately, for the range of physical conditions that will be studied, lower than ~ 0.004 .

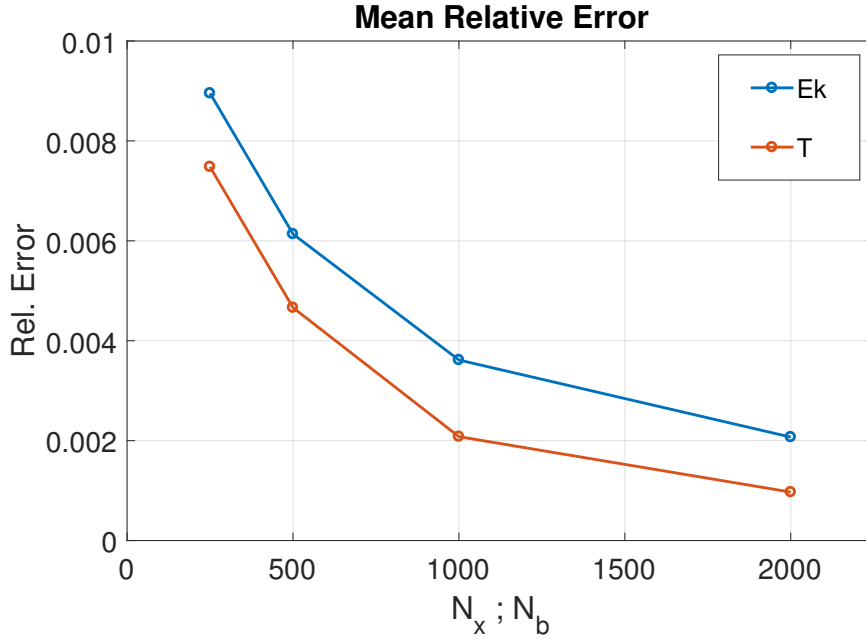


Figure 4.1: Mean relative error of the kinetic energy and temperature solutions when duplicating the number of nodes in both spatial (N_x) and beam (N_b) discretizations. Experiment with a Deuterium-Tritium plasma at 1 keV and $\rho = 300 \text{ g/cm}^3$, with a proton beam of $Ek_0 = 3 \text{ MeV}$ and $Q = 0.75 \text{ GJ/cm}^2$

$N_x = N_b :$	250	500	1000	2000
Time (s)	16	65	320	1335

Table 4.1: Computational time required using each number of nodes

On the other hand, in figure 4.2 it is shown the final temperature (of the heating process) as a function of the depth, with different discretizations of the beam (N_b). This allows to observe how the discretization of the temperature equation influences the results. It can be observed that when the number of bins is increased the solution converges, however, when the number of bins is not enough, the solution oscillates and has a peak for every bin.

This figure makes allusion to the section 3.2.2, where is explained that if the refinement of the beam discretization in bins is not precise enough, it will not simulate the beam smoothly, instead of separated projectiles.

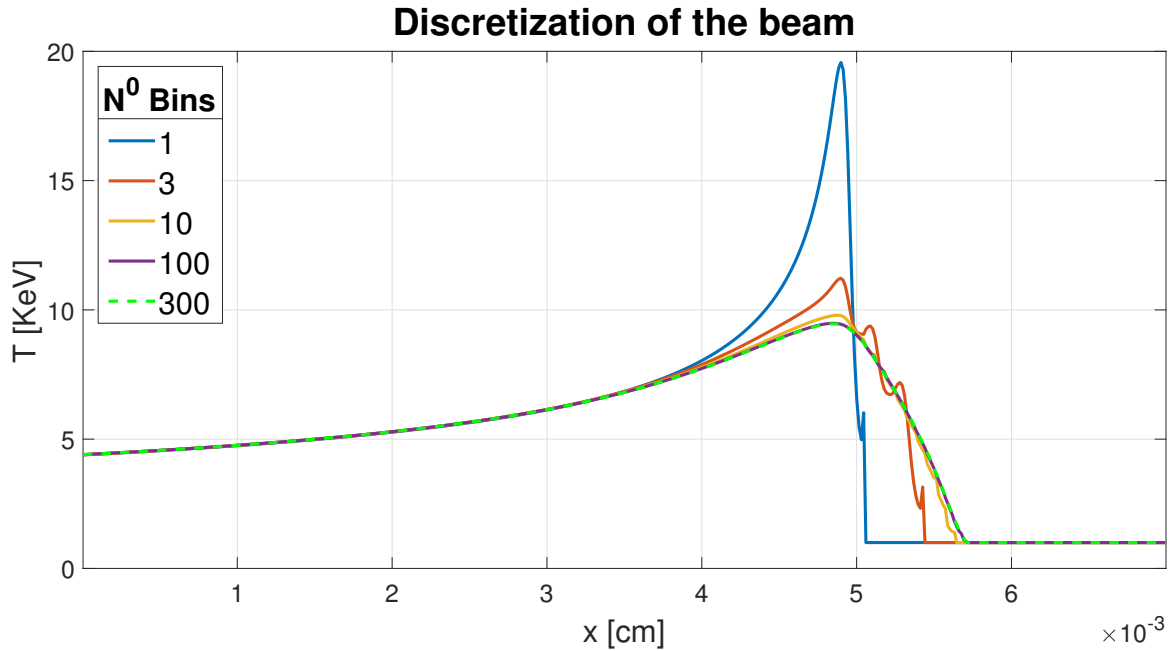


Figure 4.2: Spatial distribution of the temperature of the plasma when the beam has been discretized in a number of bins. Experiment with a Deuterium-Tritium plasma of $\rho = 300 \text{ g/cm}^3$ at 1 keV and a Vanadium beam with $Ek_0 = 5.1 \text{ GeV}$ and $Q = 1 \text{ GJ/m}^2$.

4.1.2 Adaptive Mesh

In this work, the adaptive mesh method presented in section 3.1.4 has been implemented in STOPBIN code only to solve the kinetic energy equation. The numerical experiment is done with an Aluminum plasma at 50 eV and a proton beam with 1 MeV of initial kinetic energy.

In the left frame of figure 4.3 is shown how an adaptive mesh solves the kinetic energy equation. The initial mesh had 50 nodes and was refined until the relative error per node is lower than $\tau = 1e^{-5}$. After the refinement process the number of nodes has augmented as it can be observed in the figure. Moreover, in the regions where the slope increases the number of nodes is higher, as it is observed when the beam has low kinetic energy values.

In the right frame, the stopping power is evaluated in the same adaptive mesh. The results found corroborate the mesh discretization of the kinetic energy, for instance, in the region where the stopping falls straightly, the adaptive needs more nodes to fulfill the threshold condition. The nodal jump found in this frame comes from the fact that the adaptive mesh is calculated over the error in the kinetic energy Ek , not with the stopping power values. On the other hand, the stopping power drops straightly when the projectiles have lost its energy so there is truly unnecessary to find nodes in this region.

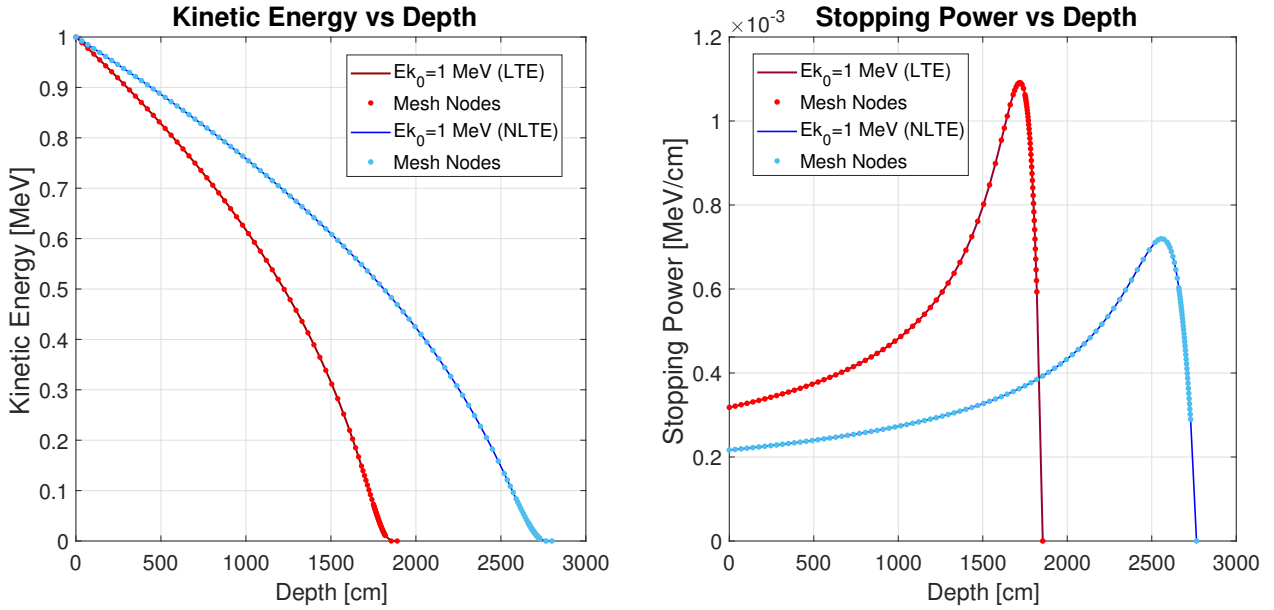


Figure 4.3: Kinetic energy (left) and stopping power ($S_{p_{free}} + S_{p_{bound}}$) (right) vs. depth for an Aluminum plasma at $T = 50 \text{ eV}$, $n_{at} = 10^{16} \text{ cm}^{-3}$ and a proton beam of $E_{k_0} = 1 \text{ MeV}$, in LTE and NLTE plasma conditions. The initial mesh has 50 nodes and the tolerance threshold for the error per node is $\tau_{Ek} = 10^{-5}$.

4.2 Behavior and Comparative with other models

An external physical test is necessary to ensure that the expressions selected in section 2.2.4 to calculate the stopping have been implemented correctly and are adequate to solve the problem, i.e, making an external test. In order to check the validity of each single kind of stopping, the expressions will be solved separately (shown with solid lines) and compared with the results of other research groups (shown with dotted lines).

First, the validity of the free electron stopping power is checked. In our model an analytical approximation of the PMV free electron stopping has been selected and it is valid for classical or non degenerated plasmas, i.e, when the plasma temperature is larger than the Fermi temperature ($T > T_F$). The PMV free electron model is tested in a comparative with the RPA model [14]. Random Phase Approximation (RPA) stopping power model is valid for degenerated and non degenerated (quantum and classical, respectively) plasmas. In the left part of the figure 4.4, for an Aluminum plasma at 10^{19} cm^{-3} free electron density, it is shown the ratio between the stopping power calculated at temperature T and those calculated at reference temperature $T_0 = 50 \text{ eV}$. This ratio is presented for PMV and RPA models, and it can be seen that both ratios have similar behavior in the temperature interval between $50 - 500 \text{ eV}$, in function of the proton energy. This results provides a satisfactory test for our free electron stopping model.

In the right part of the figure 4.4, also for Aluminum plasma, we compare our bound electron stopping power model with the Local-Density-Approximation-bound (LDA-bound) stopping model [15], for a density of atoms $n_{at} = 4.45 \cdot 10^{20} \text{ cm}^{-3}$ and a temperature of $T = 4.5 \text{ eV}$. Taking into account that the atomic number of

aluminum is 13, then, at this condition, there is an important contribution of the bound electrons to the total stopping power. As it can be seen in the figure, the comparison between both stopping models shows good agreement in all range of proton energies. Moreover, this same plasma is studied in [15] with a stopping model based on the relativistic average ion-sphere model, that is more rigorous than the LDA-bound model. So, it is important to highlight that the figure 3 of this reference confirms that the behavior shown by our model in 4.4, fits suitably with the average ion-sphere stopping power model.

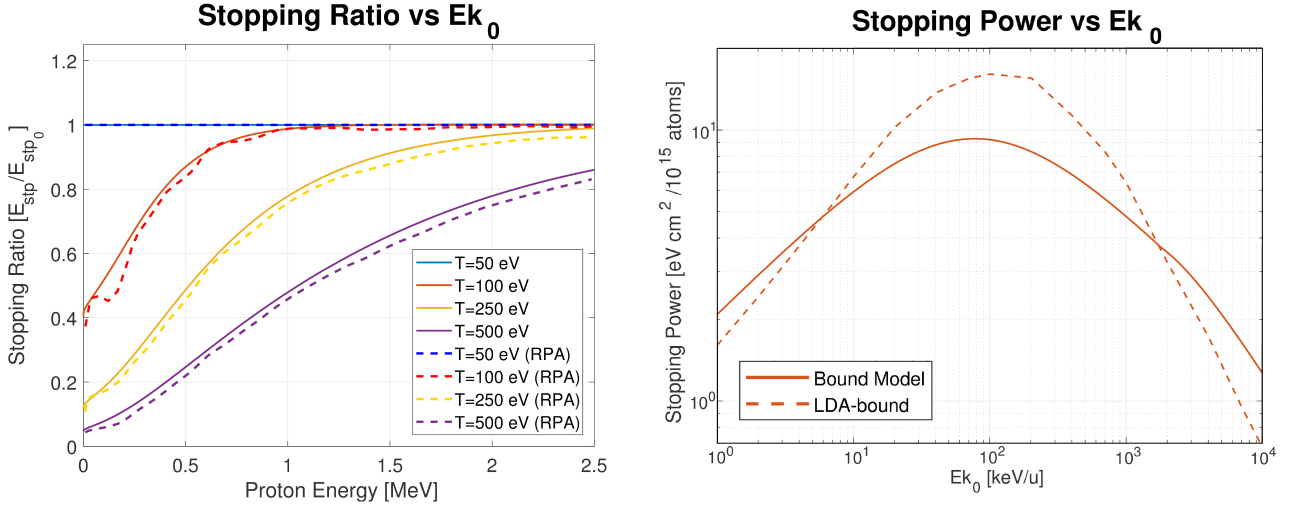


Figure 4.4: Left: PMV-RPA validation with the Stopping Ratio, for $n_{ef} = 10^{19} \text{ cm}^{-3}$ and $S_{pt_0} : T = 50 \text{ eV}$. Right: Bound electron model-LDA validation with the Stopping Power, for $T = 4.5 \text{ eV}$ and $n_{at} = 4.45 \cdot 10^{20} \text{ cm}^{-3}$.

Then, we test the free electron and ion stopping models analyzing the stopping of protons in full ionized mixture of Deuterium-Tritium (DT) plasma. The matter density and the temperature of the DT plasma are $\rho = 300 \text{ g/cm}^3$ and $T = 1 \text{ keV}$, considering the same proportion of deuterium and tritium. Additionally, the mixture of DT plasma is considered with dopant elements such as Aluminum and Copper, following the ideas developed in the reference [16]. The presence of the dopants modifies the ion stopping expression as $S_{p_{ion}} = S_{p_{ion}(DT)} + S_{p_{ion}(Dop)}$, as well as, the free electron density $n_{ef} = n_{ef}(DT) + n_{ef}(Dop) = (1 + 0.5Z_T\xi)n_{ef}$, where ξ is the dopant percentage respect to the Deuterium-Tritium abundance, that in this study is fixed at $\xi = 0.005$. In figure 4.5 the ion stopping (left) and the electron stopping (right) are shown, both for our stopping model (solid line) and the one used in the reference (dotted line), for the commented conditions above. First of all, it can be seen that the ion and free electron stopping power of protons grows up when the DT mixture has a dopant, being the growth higher when the atomic number of the dopant increases. On the other hand, the maximum value of the ion stopping is achieved at low proton energies, while for the free electron stopping it is achieved at higher energies. Moreover, this last behavior do not change when DT plasma has a dopant. Secondly, in figure 4.5 it is observed that both models share the same behavior, although, there are differences between our stopping model and the other one. The relative differences between them are at the order of 15-20 %

where the stopping is maximum, which is an acceptable discrepancy when stopping power models have been obtained under different approximations.

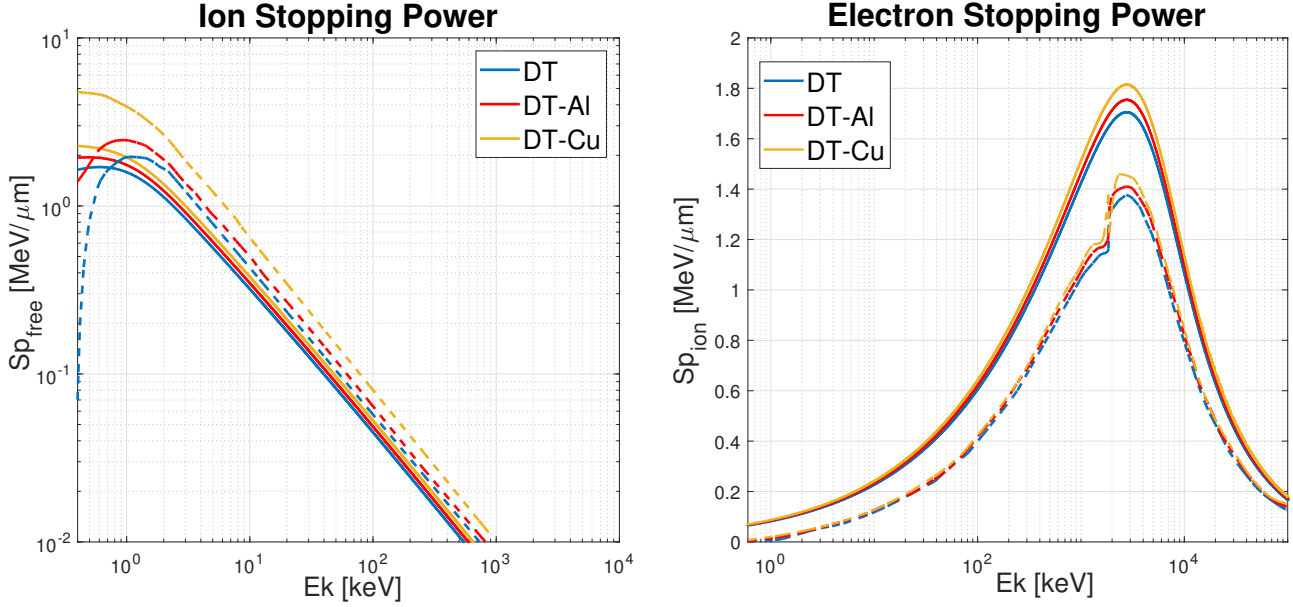


Figure 4.5: Left: Ions Stopping Power Stopping. Right: Electron Stopping Power. Both experiments for a DT plasma at a 1 keV temperature, $\rho = 300 \text{ g/cm}^3$, the dopant portion respect to the DT is $\xi = 0.005$, with different kinds of dopant and a proton beam.

Next, we check the validity of the solutions of the stopping power and the energy loss with the spatial evolution, following the expressions from the section 3.2.3. Remaining with the same DT plasma mixture at $\rho = 300 \text{ g/cm}^3$, in the figure 4.6 is shown the stopping power in function of the spatial position x , of a full ionized carbon ion beam with an initial energy of $Ek_0 = 440 \text{ MeV}$ entering in a DT plasma at different temperatures. In the figure is shown the stopping power calculated by us (solid line) and the calculated in article [17] (dotted line). The result show numerical differences but the same functional behavior. This numerical discrepancies in the curves are a result of the different stopping power expressions that our model and the authors from the reference use. A singular example of this differences, is the sharp peak that is found in the figure 4.6, which appears because the ion stopping power (Sp_{ion}) is included in our model but not in [17]. Moreover, the peak appears in the final part of each curve because the values of the ion stopping power are higher at low projectile velocities. Afterwards, we study the heating of the plasma after interacting with a certain number of projectiles. Keeping the same DT plasma ($\rho = 300 \text{ g/cm}^3$), the results of our model (solid lines) are compared with the results of the article [8] (dotted lines). The figures show the temperature of the plasma as a function of the distance multiplied by the density ρx for the last instant of the beam.

The figure 4.7 shows the change in the temperature, respect to the initial temperature of the plasma $T_0 = 1 \text{ keV}$, after the interaction with $N_{Bins} = 2000$ successive

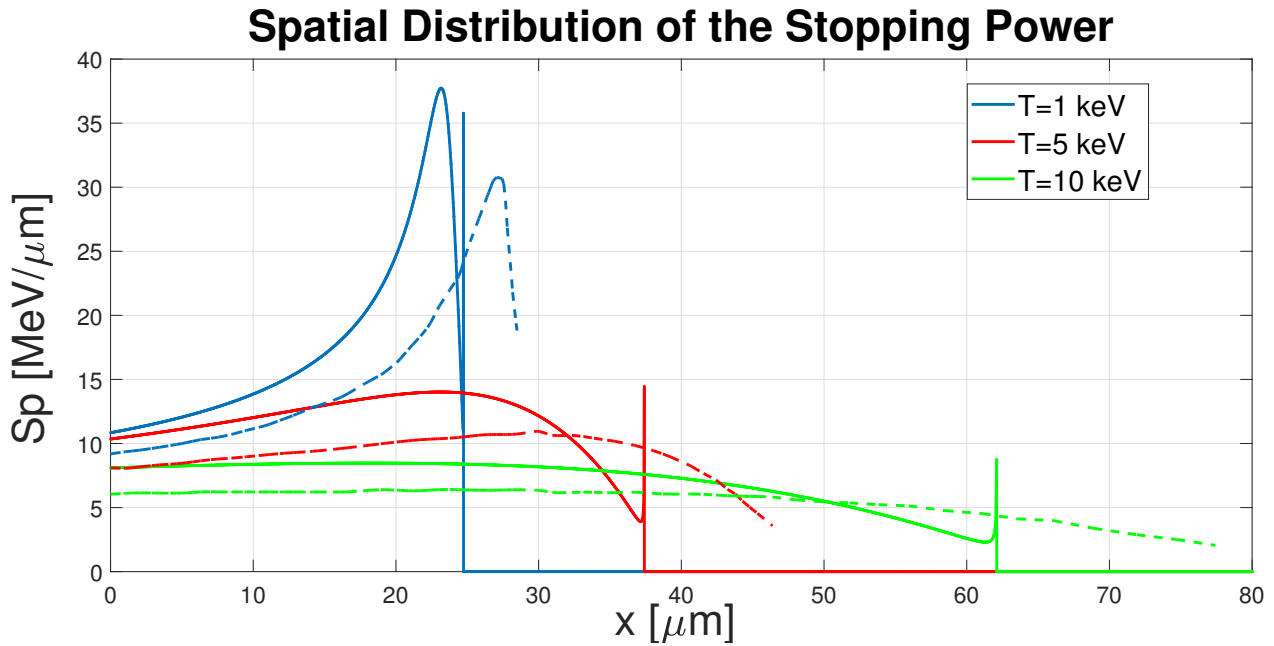


Figure 4.6: Stopping power of a bin as it deepens in the plasma. Experiment with a carbon beam with $E k_0 = 440 \text{ MeV}$ in a DT plasma with $\rho = 300 \text{ g/cm}^3$ and a T of 1, 5, and 10 keV

bins with $Q = 0.75 \text{ GJ/cm}^2$ of carbon ion beam at various initial ion energies. As expected, the plasma temperatures are higher than the initial one, moreover, the temperature distribution is not constant and it is found that the first regions of the plasma have higher temperatures than the final regions. This is a consequence of the bin not depositing the same energy in each position, and indicates that its energy drops while traveling through the plasma, as the temperature is lower in the regions where the projectile has less energy.

Similarly, in figure 4.8 there are shown the results of the spatial distribution of the temperature, when a vanadium ion beam enters the plasma with an initial kinetic energy of $E k_0 = 5.1 \text{ MeV}$ and several energy flux values Q . Unlike the previous case, in this figure it is found that the plasma has the maximum temperature at $\rho x = 1.45 \text{ g/cm}^2$ for all the three curves. This indicates that in the experiment, the mayor deceleration of the bin happens in this region, so the projectile loses more energy and the temperature of the plasma rises higher.

In figure 4.7 the three curves calculated with our model show differences with the curves of the reference. This discrepancies appear because of using different stopping power models, but a similar behavior is found among them. In figure 4.8 the reference results and our curves fit satisfactorily, so in this range of energies, both models approximate the stopping similarly. After comparing the results of the final temperature of the plasma, we can conclude that the heating model of section 3.2.3 works properly.

In general, we can conclude that the results of our model in comparative with the different experiments of other authors share the same functional behavior but show numerical differences. This numerical discrepancies in the curves are due to the different stopping power expressions that each author uses.

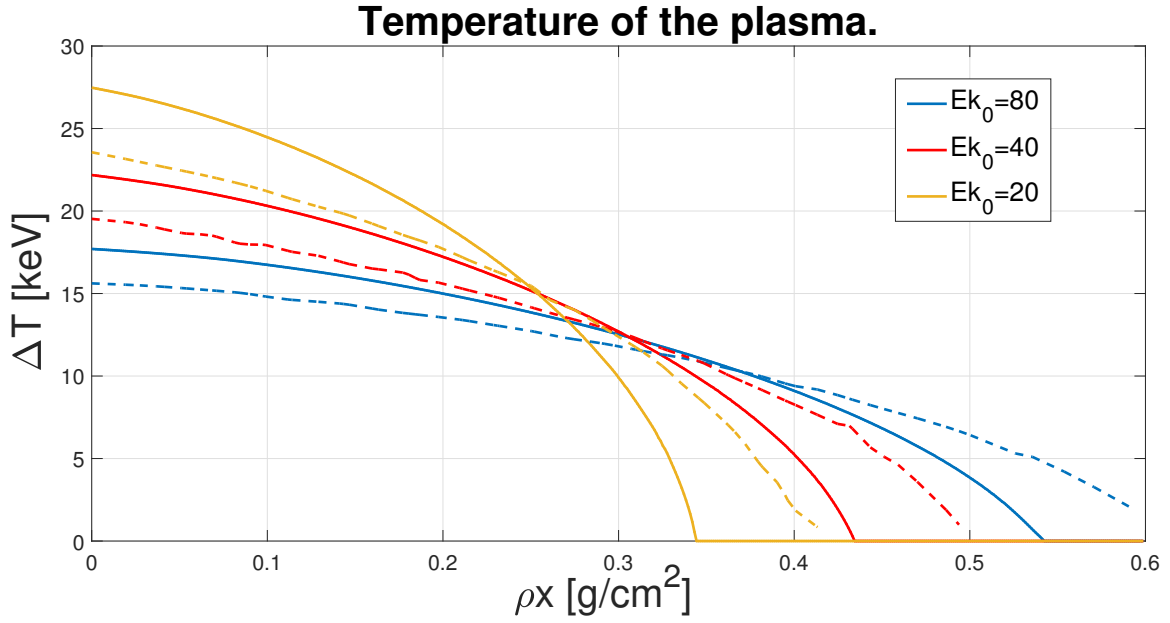


Figure 4.7: Temperature increment ' ΔT ' after a heating by a carbon ion beam of specific energy flux $Q = 0.75 \text{ GJ/cm}^2$ at various initial ion energies 80, 40, and 20 MeV, with a DT plasma of $\rho = 300 \text{ g/cm}^3$ and $T_0 = 1 \text{ keV}$.

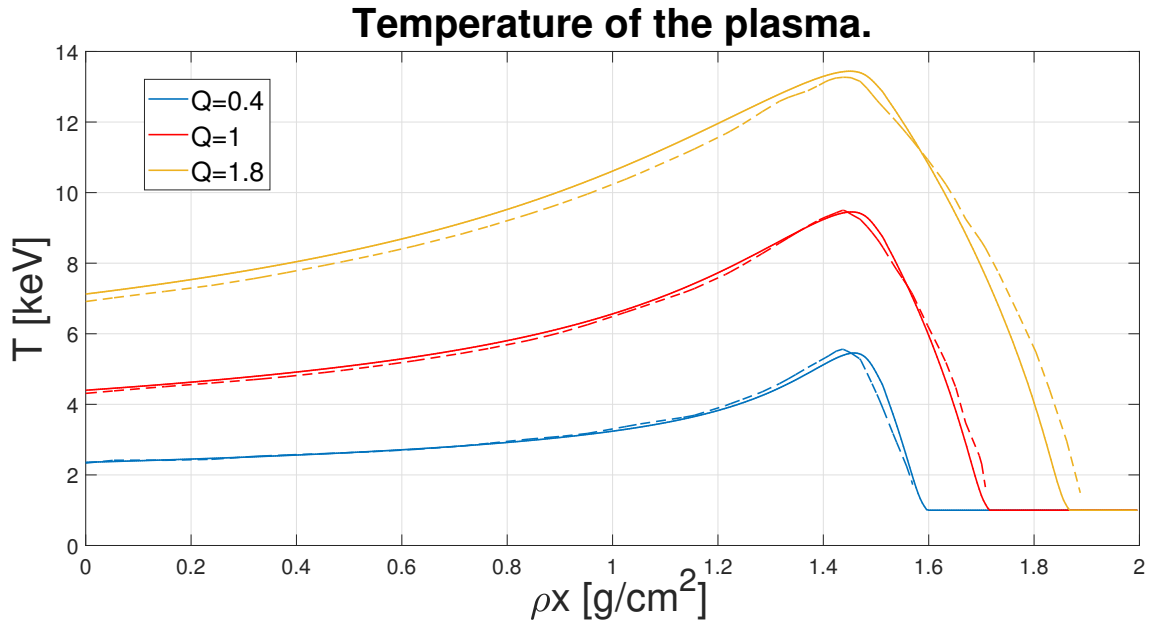


Figure 4.8: Heat-up by a vanadium ion beam of energy $E_0 = 5.1 \text{ GeV}$ at various specific energy flux values $Q = 0.4$, $Q = 1$, and $Q = 1.8 \text{ GJ/cm}^2$, with a DT plasma of $\rho = 300 \text{ g/cm}^3$ and $T_0 = 1 \text{ keV}$.

4.3 Experiments

Once the physical and numerical model proposed in this work has been tested, in this section we propose a set of experiments to simulate using the STOPBIB code. This allow us to show the capabilities of the code and to study the behavior of the ion beam interaction processes for some situations of interest in the field of the

laboratory experiments or in the fast ignition. In the figure 4.9 is shown the range of conditions used to frame our experiments.

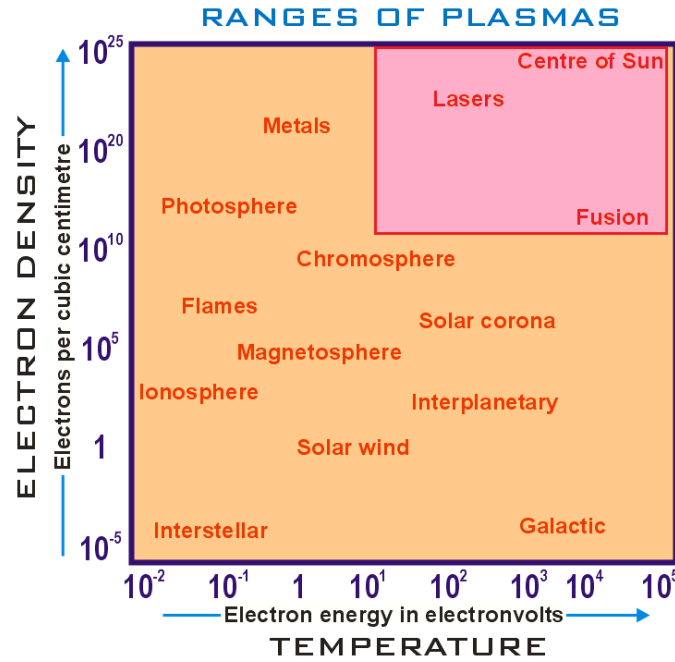


Figure 4.9: Range of temperature and electron density where the experiments are performed.

4.3.1 Proton Beam in an Aluminum Plasma

Aluminum plasma is a common target in the theoretical and experimental researches of this field [18]. Analyzing the interaction between a proton beam and an Aluminum plasma target, is a good starting point to understand the general behavior of the interaction between an ion beam and a plasma, so there will be an study of the stopping power and the kinetic energy as a function of the depth, as well as, the range of the beam. This last one, is defined as the maximum depth achieved by the ions in the plasma, according to the deposition of the energy.

In these simulations, we have focused in the study of the influence of the thermodynamic regime in the beam-plasma interaction processes. MIXKIP code can solve the rate equations or Saha-Boltzmann equations to calculate the ion populations of the plasma for different plasma conditions. However, Saha-Boltzmann equations are only valid when the plasma is in the LTE thermodynamic regimen, and in this situations, rate equations and Saha equations provide the same results. In this analysis, the calculations to determine the ion populations obtained from rate equations are labeled as NLTE while those obtained from Saha-Boltzmann equations, as LTE. Same criteria is used with the stopping power or energy deposition calculation when the output data from MIXKIP code are required.

As is well known, a plasma achieves the LTE when the density increase or the temperature decrease. For this reason, we have selected relatively low values of the atomic density ($10^{16} - 10^{20} \text{ cm}^{-3}$) and temperature in the range given by 10 – 50 eV, because in this ranges the aluminum plasma can be found in LTE and NLTE

thermodynamic regime. On the other hand, at these plasma conditions, the average ionization of the Aluminum plasma goes from 2.5 to 13, i.e, the bound electrons in the plasma go from 11.5 to fully ionized aluminum plasma. Therefore, it can be analyzed the stopping power contribution of the bound electrons, free electrons and ions.

This contributions are shown in the figure 4.10 (top) for an ion proton beam with initial kinetic energy of 0.05 MeV and an Aluminum plasma with $\rho = 10^{16} \text{ cm}^{-3}$ and $T = 10 \text{ eV}$. At this plasma condition, MIXKIP code provides an average ionization of 3.06 (or an average number of bound electrons of 12.06) and a mean excitation energy of the bound electrons of 350 eV , calculated with 5786 atomic levels for the collisional-radiative simulation. In figure 4.10 (top) it is observed that the stopping power value is mainly determined by the stopping of free electrons (so it is taken as a reference). Meanwhile, the bound electrons make small contributions to it, and the ion stopping does only happen at low energies or velocities, but with a stopping power peak that stops the projectile at a sudden. Therefore, the main effect of the ion and bound electrons is to reduce the range of the proton in the plasma. In the figure 4.10 (bottom) it is shown the kinetic energy of the projectile, and as expected, the proton decelerates as dives in the plasma, so its kinetic energy will fall with the distance traveled. In the figure 4.11, which is similar to figure 4.10, the temperature of the Aluminum plasma is $T = 50 \text{ eV}$, and it is observed a similar behavior than at $T = 10 \text{ eV}$. In this case, the average ionization increases $\bar{Z}_T(T = 50) > \bar{Z}_T(T = 10)$, and therefore, the bound electron stopping contribution decreases and the free electron stopping rises. Thus, comparing figures 4.10 and 4.11, it is found that the bound electron stopping power has a larger contribution to the free electrons stopping when the plasma has a temperature of $T = 10 \text{ eV}$. However, in spite of finding a greater number of free electrons at $T = 50 \text{ eV}$, in the figures it is observed that the stopping power at 50 eV is lower than at 10 eV , while the range or maximum distance traveled is greater. This results are found because, in general, the stopping power (as a function of the energy of the projectile) decreases when the temperature arises.

In the figure 4.12 (top) it can be observed the influence of the thermodynamic regime of the target plasma in the stopping and energy deposition of the projectile. It has been simulated the proton beam with an initial energy of 0.5 MeV , entering in an aluminum plasma with an atomic density of 10^{16} cm^{-3} and temperatures of 10 and 50 eV . Due to the low density, the aluminum plasma is in NLTE thermodynamic regime. For example, at 10 eV , the average ionization from NLTE and LTE calculations are 3.07 and 4.47, respectively. Therefore, LTE calculation overestimates the number of free electrons in the plasma. Now, taking into account that the free electron stopping is the more important contribution to the total stopping, it can be understood that the stopping from LTE calculation is major than the NLTE one, and the corresponding range is minor. As a consequence, reverse behavior is observed in the kinetic energy of the ion, as it is shown in the figure 4.12 (bottom), where the kinetic energy of the ions is deposited in a shorter portion of plasma when it is in LTE. Similar behavior is observed for 50 eV .

In figure 4.13 it is shown how the density of a plasma at $T = 50 \text{ eV}$ affects the projectile. As the atomic density increases the range is reduced and the stopping power

values increases, specially the ion stopping, which, as expected, increases when the beam has more atoms to collide with. Moreover, the influence of the thermodynamic regime in the beam-plasma interaction processes is found when the atomic density increases, so at 10^{20} cm^{-3} , i.e, where both LTE and NLTE calculations provide the same results and the Saha equations are a good approximation.

We finish the study of the proton ion beam in an aluminum plasma, focusing on the behavior of the stopping and the range when the initial kinetic energy of the projectile varies. If the initial kinetic energies of the projectile are high, the beam will dig deeper in the plasma, as it is shown in the bottom frame of the figure 4.14. Moreover, in this figure we found a non-linear behavior, where not only the range increases with energy, but the slope increases too. This result indicates that at low energies the beam is more sensitive to the stopping than at high energies. This idea is proved analyzing the stopping power curves from the top frame of figure 4.14, where the stopping for low initial energies falls shortly after the beam has entered the plasma. Meanwhile, the stopping power for higher energies is constant until its value rises before completely dropping. At high energies the projectile deceleration does not change while traveling through the plasma, its velocity is slowed until the interaction with the plasma particles is significant, then the beam losses its energy sharply.

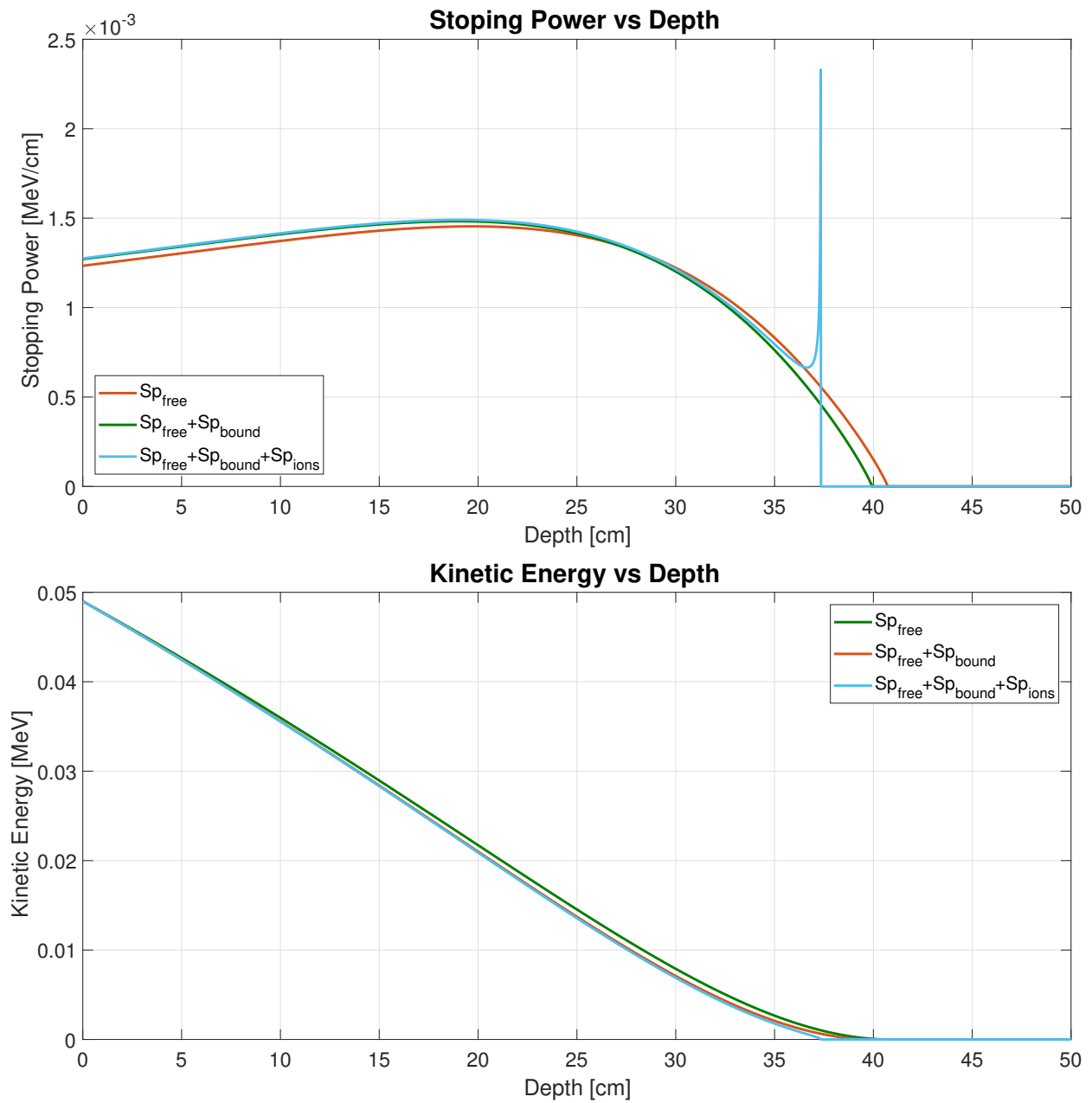


Figure 4.10: Addition of the different Stopping Power contributions (top). Behavior of the kinetic energy of the beam with the stopping power contributions. Both for a fixed atomic density $n_{at} = 10^{16} \text{ cm}^{-3}$, temperature $T = 10 \text{ eV}$ (NLTE) and a beam of $Ek_0 = 0.05 \text{ MeV}$.

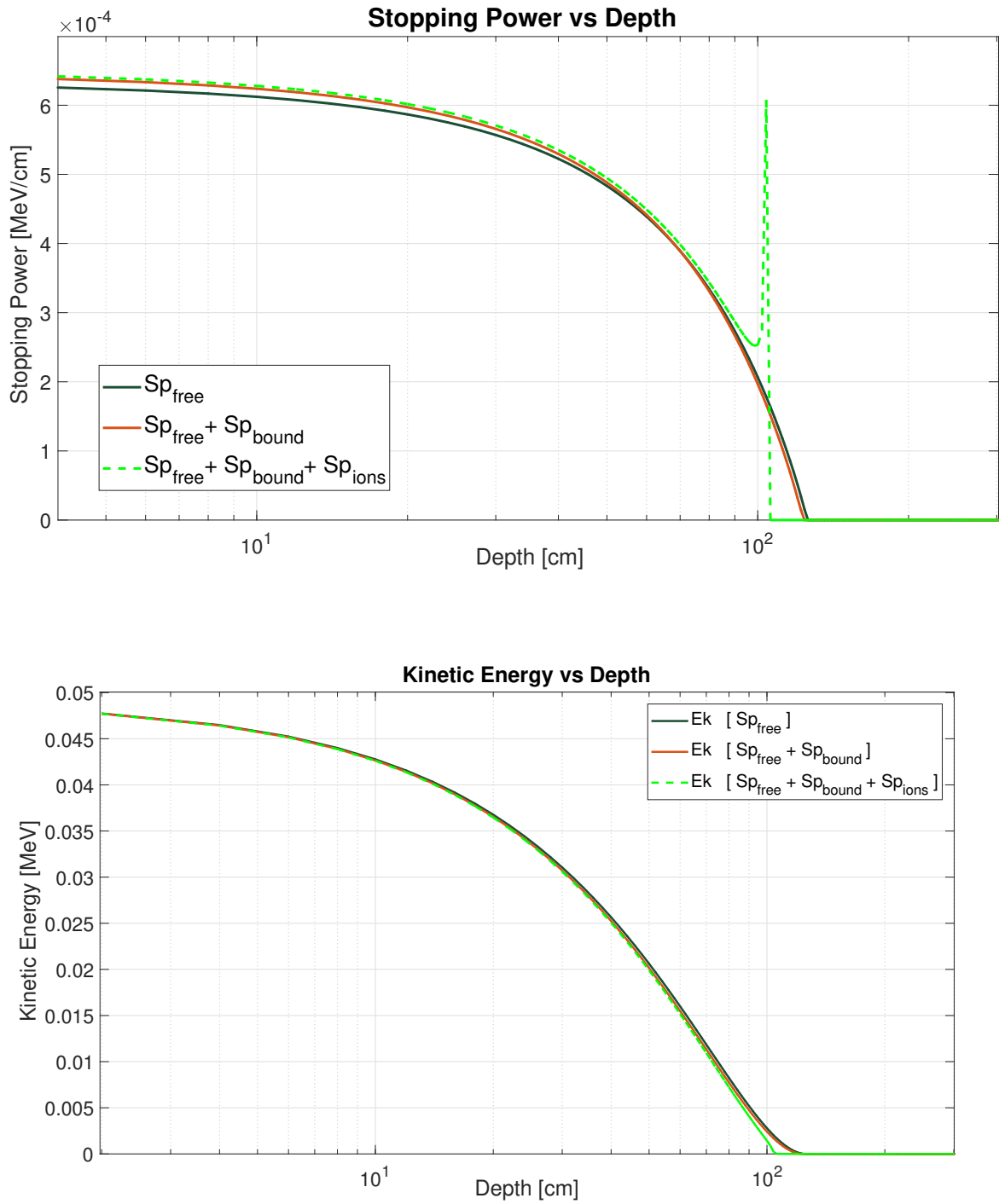


Figure 4.11: Addition of the different Stopping Power contributions (top). Behavior of the kinetic energy of the beam with the stopping power contributions. Both for a fixed atomic density $n_{at} = 10^{16} \text{ cm}^{-3}$, temperature $T = 50 \text{ eV}$ (NLTE) and a beam of $Ek_0 = 0.05 \text{ MeV}$.

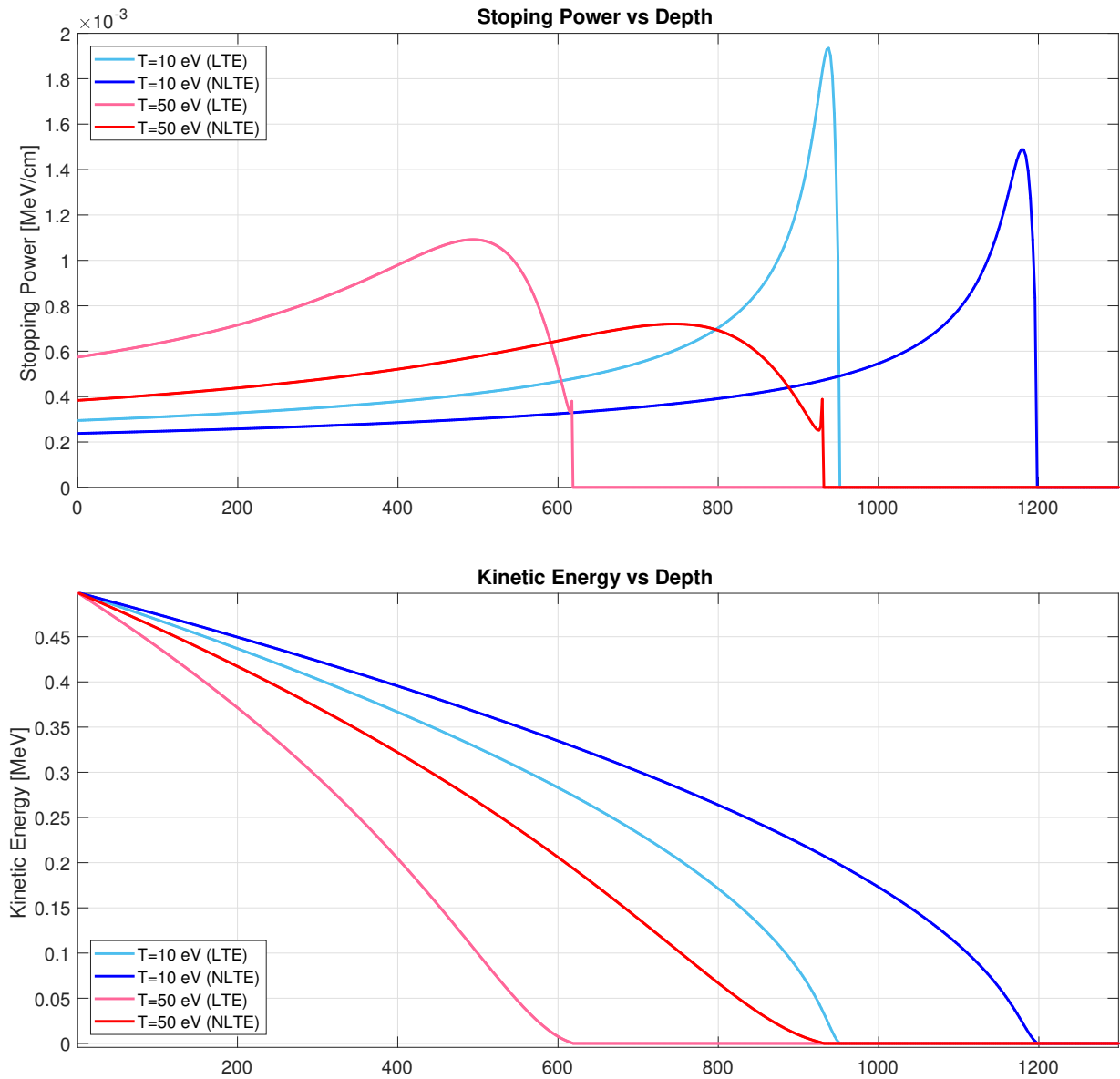


Figure 4.12: Stopping Power (top) and Kinetic Energy (bottom) dependence with depth and temperature, for a fixed atomic density $n_{at} = 10^{16} \text{ cm}^{-3}$ and $Ek_0 = 0.5 \text{ MeV}$.

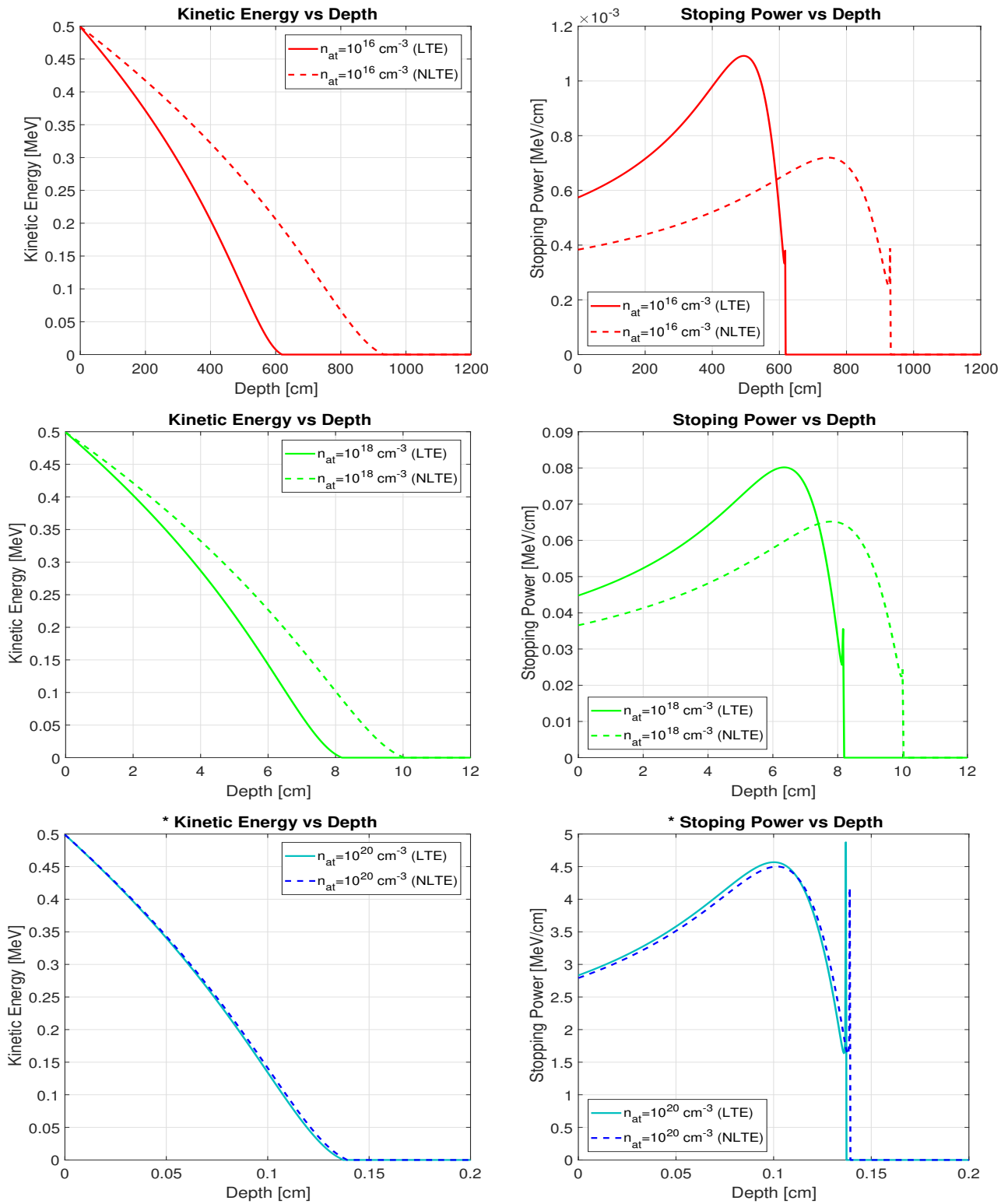


Figure 4.13: Kinetic Energy (left) and Stopping Power (right) dependence with the depth and the atomic density, for a fixed temperature $T = 50 \text{ eV}$ and $Ek_0 = 0.5 \text{ MeV}$. * Indicates that $Z_P/(n_{ef}\lambda_D^3) > 1$.

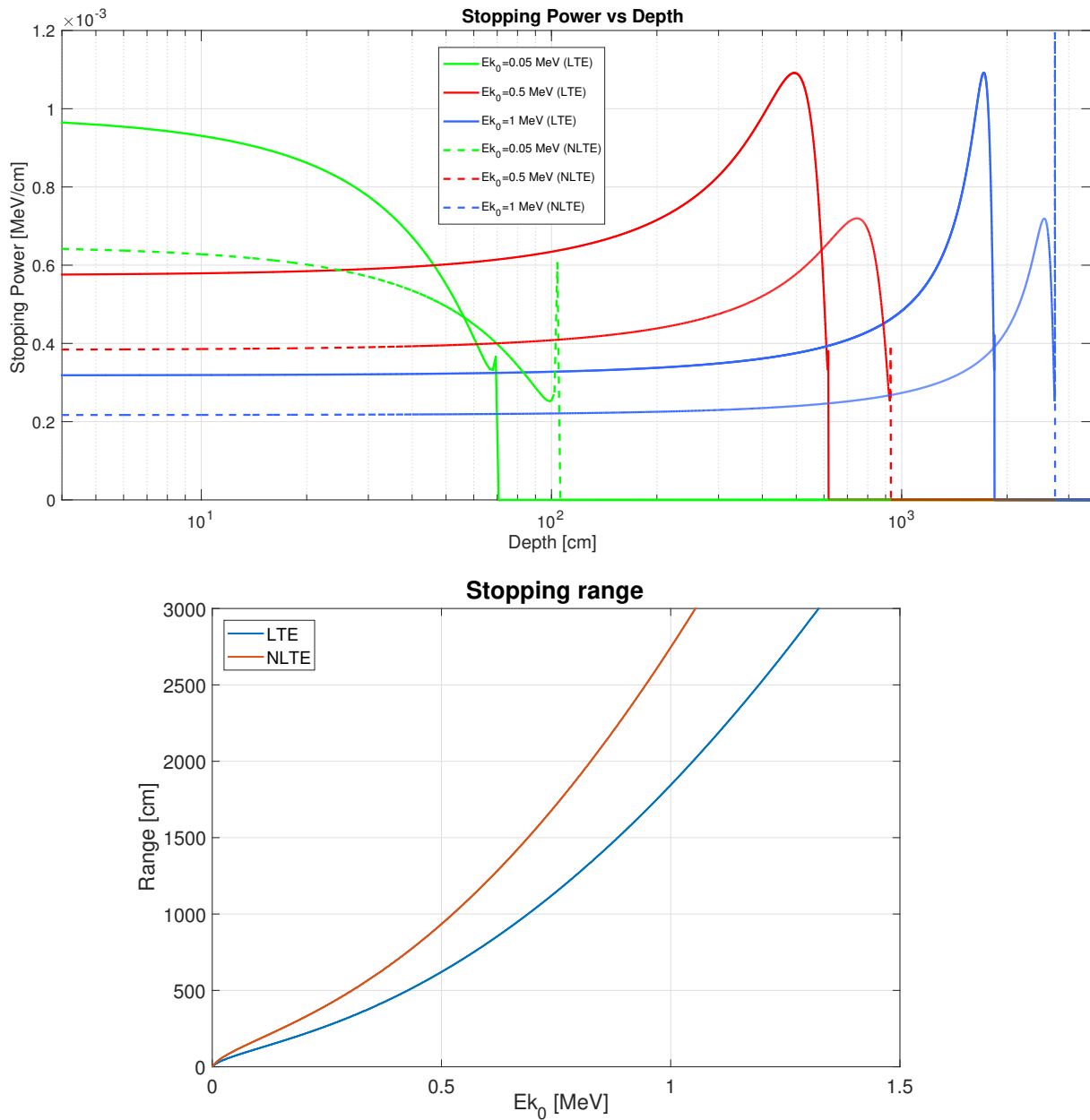


Figure 4.14: Top: Stopping Power dependence with depth and initial kinetic energy. Bottom: Range for different kinetic energies. Both for a fixed atomic density $n_{at} = 10^{16} \text{ cm}^{-3}$ and temperature $T = 50 \text{ eV}$.

4.3.2 Proton Beam in a Deuterium-Tritium Plasma

The heating by an ion beam of high energy is one of the promising methods for fast ignition of a precompressed deuterium-tritium (DT) target, in the inertial confinement fusion context. Plasma heating in fast ignition is a nonlinear process with strong feedback: an increase in temperature up to values of 10 or 20 eV results in a significant decrease of its stopping power and increase of the ion range, and the deposition of energy of the ion beam in the plasma is affected. Also, in the compression process, the matter density of the DT plasma can change from density of solid to 1000 g/cm^3 , and the temperature from 1 to 10^4 eV . Therefore, the study of the inertial confinement fusion with fast ignition by an ion beam requires a precise knowledge of the beam-plasma interaction.

In this simulations we have focused in the study of the proton beam in a DT plasma. Thereby, following the conditions of the articles [8, 17], we propose a Deuterium-Tritium plasma and a proton beam partitioned in 2000 bins, with an initial kinetic energy of $Ek_0 = 3 \text{ MeV}$ and $Q = 0.75 \text{ GJ/cm}^2$.

A detailed analysis of the figures 4.15 and 4.16, allow us to obtain detailed information about the stopping and heating process.

The first figure 4.15 shows the stopping power, the kinetic energy and the temperature in function of the distance or in function of the bins that have entered the plasma. Initially the plasma is homogeneous at $T = 1 \text{ keV}$ and the density is constant with $\rho = 200$ or 500 g/cm^3 . In the frame **F** of this figure, is shown the temperature vs. the number of bins at different points of the plasma, is observed that in a more dense plasma, the temperatures reach higher values and the projectiles have lower ranges.

The second figure 4.16 also shows the stopping power, the kinetic energy and the temperature in function of the distance or the bins. In this case, we propose an experiment applying the same beam in two equal plasmas with $\rho = 300 \text{ g/cm}^3$, with different initial temperatures $T_0 = 0.5$ and 1.5 keV . In frames **E** and **F**, is found that both plasmas reach the same temperature when all the bins have traveled through it although having different initial temperatures. This behavior indicates that, with the parameters used in this experiment, the temperature equation of section 3.2.3 and the stopping power function, are convergent for different initial values. Further study is required to broadly justify this behavior.

Moreover, the figures 4.15 and 4.16 share a great amount of information about the general behavior of the plasma and the beam. Among the results in function of the distance, it is found that the kinetic energy, the temperature and the stopping power of the first bin fall with the depth, but the stopping power of the last bin shows a constant deceleration except in its final values. On the other hand, the curves as a function of time (or number of bins), show an increase of the kinetic energy and the temperature, while the stopping power descends.

As expected, we found that the temperature of the plasma increases as the projectiles dives in it, as it is shown in the frames **F** and **E** of both figures. Moreover, it is observed a uniform increase in the temperature in most of the plasma, except in the final region, where the temperature falls to the initial temperature. Therefore, the properties of the plasma will change with the temperature and the deceleration of

the projectiles will vary. Thus, when the plasma is heated the stopping power values descends with the time, as it is observed in the graphics **D**. This last result is also observed in the figures **C**, where the first bin (plasma at initial temperature T_0) has more stopping than the last one (heated plasma $T > T_0$). This behavior indicates that under this conditions, the stopping power is descends when the temperature rises.

As the stopping power is higher for low temperatures the projectile will have a shorter ranges. For instance, in graphic **A** it is shown the energy loss of the beam and we can observe that the first bin has a much shorter range (the plasma is at T_0) than the last bin ($T > T_0$).

In figures **B**, **D** and **F** it is found that a certain number of the first bins that enter the plasma have null values in the $L/4$ region of the plasma. This happens because neither of these bins has deepened that far. However, as the plasma heats up, the range of the bins increases and at some point they will reach the $L/4$ region. Thus, when a bin reaches a region that is still at the initial temperature, the stopping is large. But, once the region is heated by the successive bins, the stopping power decreases in this region. That justifies why the stopping power of the first bin that enter a region at T_0 is higher than the stopping of the last one.

In figure **D** it is observed that when a large numbers of bins have traveled through the plasma, the stopping power value of all the curves reaches a similar value and that the slope is low, i.e, when the plasma has been already heated up, the stopping power does not vary significantly. This result is related with curve of the last bin of the figure **C**, where the stopping power shows a constant behavior in the regions of the plasma that had been heated up, and a sharp peak where it is still at lower temperatures

In figures **B**, it is found that all the bins at $x = 0$ have the same energy, although the plasma has been heated up. This result is observed again in the graphic **A**, where the kinetic energy does not vary for the first bin in the positions nearby positions to $x = 0$ of the plasma.

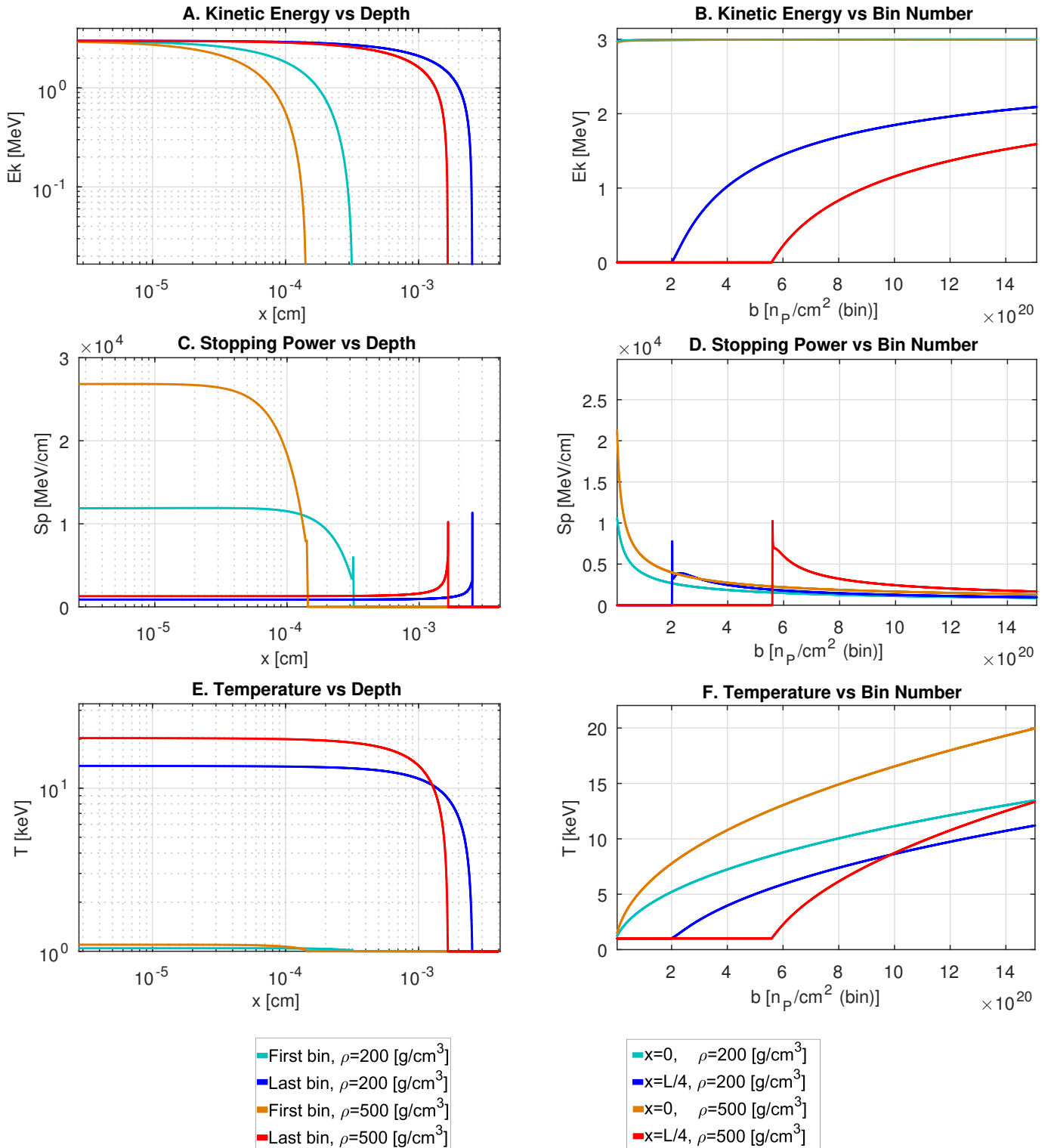


Figure 4.15

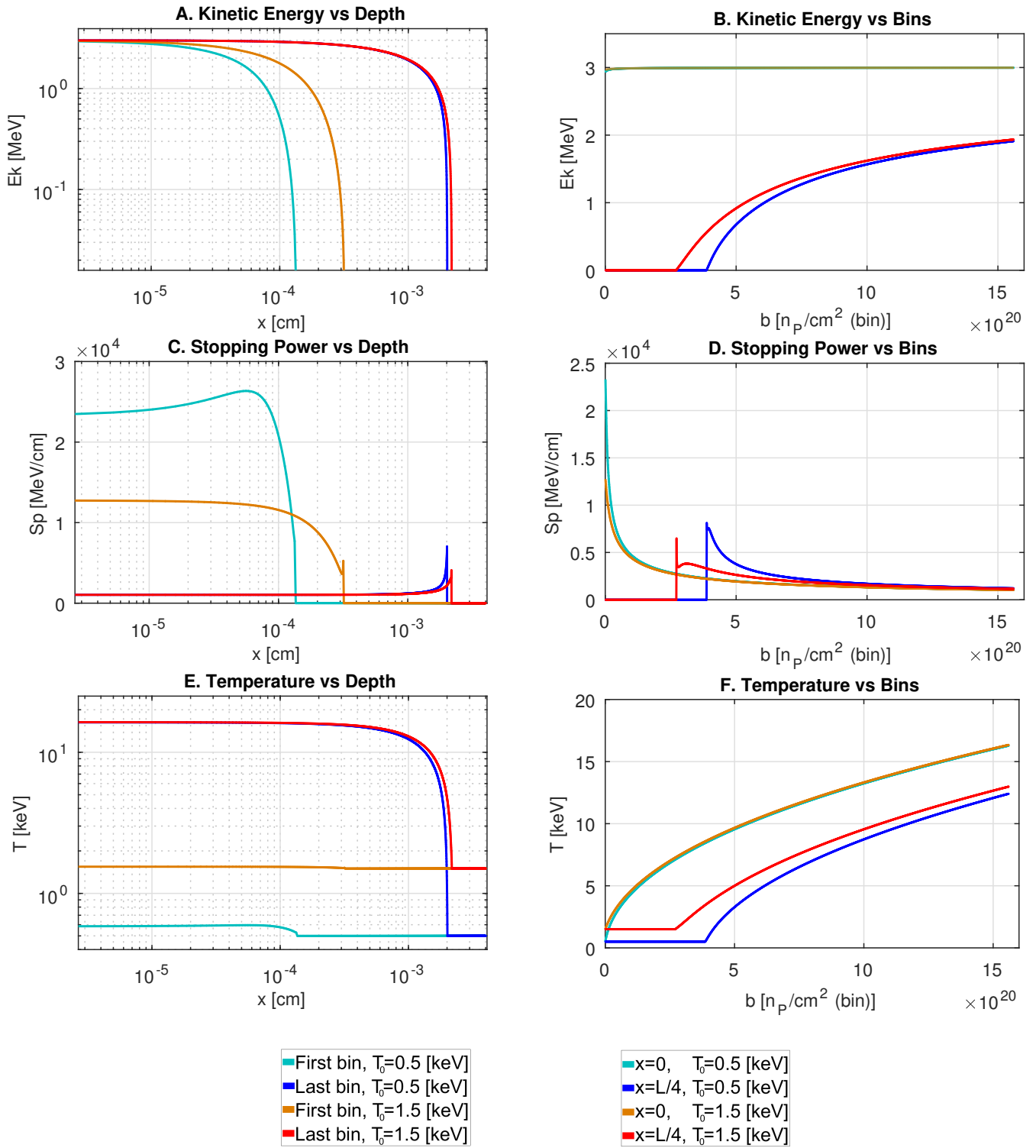


Figure 4.16

Chapter 5

Conclusions

This work focus in developing a theoretical and computational model for the simulation of the interaction of an ion beam in a plasma in a wide range of conditions. The simulation return space-time results of the stopping power, kinetic energy of the beam and temperature of the plasma. Simulations of the beam-plasma interaction for different conditions have been presented, studying the behavior of the stopping power, the energy loss of the beam, the range and the change of the temperature field.

The main goals of this work that have been achieved are:

- It has been learned the main concepts of the plasma physics necessary to study the ion beam-plasma interaction process and the methodology to approach a physical problem from a computational point of view.
- The principal approaches to the description of a plasma have been studied. Among them, it has been studied the collisional-radiative model and how it is simulated in the MIXKIP code in Fortran programming language.
- It has been developed a physical and numerical model for the study of the beam-plasma interaction in a wide range of conditions of densities and temperatures, plasmas with different chemical components (monocomponent, multicomponent and dopants), as well as ion beams with a large range of initial energies and various chemical components for the beam.
- The physical and numerical model have been implemented in the computational code STOPBIN. The code is written in Matlab environment, taking advantage of its computational features, in order to reduce the computational cost and exploit the possibilities in the calculation. Moreover, STOPBIN code includes an adaptive mesh and the estimation of the error.
- STOPBIN code is capable of solving the equations that govern the kinetic energy projectile and the heating of the plasma. Moreover, STOPBIN code has been develop to carry out a multiparametric analysis.

- Using STOPBIN code, it has been performed numerous simulations of the ion beam-plasma interaction for different physical conditions. The results of the simulation are compared with the researches of other authors under some conditions, finding a good agreement between them. The results of the simulation have been analyzed in order to understand the behavior of the beam-plasma interaction.

5.1 Future Lines of Work

This TFM leaves open the possibility to extend the work in the future. To begin with, it would be of interest to perform a deep parametric analysis of experiments in the range of values that are used in the fast ignition process of nuclear fusion plant. Thus, the ignition process could be characterized for different ion beams and plasma conditions.

On the other hand, in this work was studied a beam with a short pulse time. STOPBIN code could be extended to study a beam with a pulse time similar to the hydrodynamic time of each process, so it will be necessary to modify the plasma heating model in order to include this plasma processes. If the conduction process is included, it will be possible to simulate the heat propagation due to the interaction with the beam. This simulation could be performed in two or three dimensions, in that case the problem will be studied with a finite elements method. Also, the internal structure of the projectile ions could be considered, i.e, studying a non point-like beam. This would lead to find a new, more accurate, expression for the stopping power function in the case of a multielectronic ion beam.

Besides, the STOPBIN and MIXKIP codes could be connected by using the temperature outputs of STOPBIN as inputs of MIXKIP, therefore studying the change in the populations as the plasma heats up. This a very tough task from a computational point of view, so a deep previous analysis must be performed. Also, STOPBIN code could be improved by implementing the adaptive mesh method in the calculation of the temperatures. Finally, the rate equations explained in the Appendix, which have been develop particularly to be included in the MIXKIP framework, could be implemented computationally in a future work.

Appendix

In this appendix are explained the rate processes that must be included in the collisional-radiative model when a beam interacts with the plasma, in particular for the MIXKIP code. The ion beam-ion plasma interaction processes must be taken into account, in particular the ion-ion collision and charge transfer. The list of index that is used in this Appendix follows:

Index List

- i, j : initial and final state of the projectile (P)
- l, m : initial and final state of the target (T)
- ϵ : (kinetic) energy of a free electron
- K : Relative kinetic energy of the projectile mass center
- ζ, q : charge of the target and the projectile, respectively
- E : Energy of a state

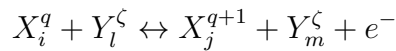
At first, the i, j or l, m subscripts will be accompanied with a P or T superscript to help the reader remember the association between the projectile and target indexes.

Ionization by Ion-Ion collision

One of the first process to study is the removing of an electron from the n^{th} shell of ion of the beam, by target ion impact. The energy balance equation of this process is:

$$E_{i,q}^P + E_{l,\zeta}^T + K_i^P = E_{j,q+1}^P + E_{m,\zeta}^T + K_j^P + \epsilon$$

And the reaction:



The initial idea to approach the rate expression is taken from the article [2], which takes both, projectile and target clouds, as a average atom approximation. So, the cross-section is expressed as:

$$\sigma_{IIC} = \sum_n N_n \sigma_n(Z^T, U_n, V_p)$$

where N_n is the number of electrons in the last (n^{th}) shell of the projectile, U_n is their binding energy (for each one of the shells of the single configuration of the

projectile average atom), V_p is the average velocity of the projectile and Z^T is the charge of the target average atom. Moreover, as the target is static in this model, it is possible to consider a distribution for the different velocities of the projectile $f(V)$ to calculate the rate:

$$\omega_{IIC} = n^T \int_{V_1}^{V_2} \sigma_{IIC}(V) \cdot V \cdot f(V) dV$$

Being n^T the total ion density of the ion plasma. If $f(V) = \delta(V - V_p)$, the rate will be:

$$\omega_{IIC} = V_p n^T \sigma_{IIC}(V_p)$$

This work proposes a detailed description of the ions, considering different charge states and atomic levels, i.e, neglecting the average atom approximation. Therefore, it will be necessary to rewrite the previous cross-section equation. First, the density of the plasma target n^T will be different for each (initial) ion charge and atomic level, expressed with the ζ and l indexes, so it is necessary to write the expression in terms of the level population $n_{l,\zeta}^T$ and the charge Z_ζ^T , both of the target ions. Moreover, N_n is rewritten as N_i and U_n will be substituted by $E_{ij,q}$, i.e, the energy difference between the energy of the initial and the final ionized state, $E_{ij,q} = I_q - E_{i,q} + E_{j,q+1}$ of the projectile. Therefore, the previous rate expression now is expressed for each consider transition as:

$$\omega_{IIC,(i,q) \rightarrow (j,q+1)} = V_p \sum_{\zeta} n_{\zeta}^T \sigma_{IIC}(Z_{\zeta}^T, E_{ij,q}, V_p)$$

That can be written using an averaged rate coefficient as:

$$\omega_{IIC,(i,q) \rightarrow (j,q+1)} = n^T \sum_{\zeta} \frac{n_{\zeta}^T}{n^T} \cdot V_p \sigma_{IIC}(Z_{\zeta}^T, E_{ij,q}, V_p) = n^T \langle \overline{V_p \sigma_{IIC}} \rangle$$

So now, the cross-section is described as:

$$\sigma_{IIC} = N_i \pi \frac{Z_{\zeta}^T e^2}{E_{ij,q}} \cdot G\left(\frac{V_p}{V_{ij,q}}\right)$$

with:

$$G(V) = \frac{\alpha^{3/2}}{V^2} \cdot \{\alpha + 2/3(1 + \beta) \ln(2.7 + V) \cdot (1 - \beta)(1 - \beta^{(1+V^2)})\}; \text{ for } V > 0.206$$

or

$$G(V) = \frac{4V^4}{15}; \text{ for } V > 0.206$$

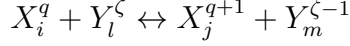
where $V_{ij,q} = \sqrt{2E_{ij,q}/m}$, $\alpha = V^2/(1 + V^2)$ and $\beta = 1/(4V(1 + V))$.

Charge transfer

In partially ionized targets, a bound electron can jump from a target ion to the projectile, i.e, capture of bound target electrons. The energy balance equation of this process is:

$$E_{i,q}^P + E_{l,\zeta}^T + K_i^P = E_{j,q-1}^P + E_{m,\zeta+1}^T + K_j^P$$

And its associated reaction:



Again, the idea is taken from the article [2], which takes both, projectile and target clouds, as a average atom approximation and using the OBK Theory [19] in first Born approximation for the Coulomb potential $-e^2/r$ and hydrogenlike wave functions (Laguerre polynomials), over the (l, m) initial and final states. The cross section is expressed as:

$$\sigma_{CT} = 4.1 \cdot 10^4 \sum_{n_i} \sum_{n_f} N_i a_{eik} \frac{(Ze^2)^2 E_i^{5/2} E_f^{3/2} E_k^4}{(E_k^2 + 2E_k(E_i + E_f) + (E_i - E_f)^2)^5}$$

where E_i and E_f are the binding energies of the electron initial (target) and final (projectile), Z is the charge state of the projectile, which has $E_k = mV_p^2/2$, then a_{eik} is taken as one, but generally is defined between $0.1 < a_{eik} < 0.4$.

Again, this work proposes a detailed description of the ions, considering different charge states and atomic levels. Instead, E_i of the target will be fixed and will be expressed as $E_{lm,\zeta}^T$, such as there is a sum over the energies of $E_{i,\zeta}^P$ and $E_{m,\zeta+1}^P$ for each charge number ζ . Then, the expression for the cross-section will be:

$$\sigma_{CT} = 4.1 \cdot 10^4 N_{l,\zeta} a_{eik} \frac{(Z_{q,i}^P e^2)^2 E_{lm,\zeta}^{5/2} E_{ij,q}^{3/2} K^4}{(K^2 + 2K(E_{lm,\zeta} + E_{ij,q}) + (E_{lm,\zeta} - E_{ij,q})^2)^5}$$

The rate is:

$$\begin{aligned} \omega_{CT,(i,q) \rightarrow (j,q-1)} &= \\ &= V_p \sum_{\zeta} \left(\sum_{l(\zeta)} \sum_{m(\zeta+1)} n_{l,\zeta}^T 4.1 \cdot 10^4 N_{l,\zeta} a_{eik} \frac{(Z_{q,i}^P e^2)^2 E_{lm,\zeta}^{5/2} E_{ij,q}^{3/2} K^4}{(K^2 + 2K(E_{lm,\zeta} + E_{ij,q}) + (E_{lm,\zeta} - E_{ij,q})^2)^5} \right) \end{aligned}$$

And the rate expressed as an average of the rate coefficients is:

$$\omega_{CT,(i,q) \rightarrow (j,q-1)} = n^T \sum_{\zeta} \left(\sum_{l(\zeta)} \sum_{m(\zeta+1)} \frac{n_{l,\zeta}^T}{n^T} \langle V_p \sigma_{CT} \rangle \right)$$

Where:

$$\langle V_p \sigma_{CT} \rangle = n^T \cdot 4.1 \cdot 10^4 N_{l,\zeta} a_{eik} \frac{(Z_{q,i}^P e^2)^2 E_{lm,\zeta}^{5/2} E_{ij,q}^{3/2} K^4}{(K^2 + 2K(E_{lm,\zeta} + E_{ij,q}) + (E_{lm,\zeta} - E_{ij,q})^2)^5}$$

Reverse ion-ion collision: Detailed balance

The detailed balance equations are found considering the microscopic reversibility of the atomic processes. Therefore, the inverse expression of the Ion collision can be found through the expression:

$$n_{i,q}^P n_{l,\zeta}^T \omega_{IIC,(i,q) \rightarrow (j,q+1)} = n_{j,q+1}^P n_{m,\zeta}^T n_e \omega_{RIIC,(j,q+1) \rightarrow (i,q)}$$

Using the Saha-Boltzmann equations, after some straightforward manipulations, the reverse ion-ion collision is expressed as:

$$\omega_{RIIC,(i,q+1) \rightarrow (j,q),\zeta} = \left[2 \left(\frac{2\pi m_e T}{h^2} \right)^{3/2} \frac{g_{j,q+1}^P g_{m,\zeta}}{g_{i,q}^P g_{l,\zeta}^T} e^{(E_{l,\zeta} - E_{m,\zeta})} \cdot e^{-E_{ij,q}/kT} \right]^{-1} \cdot \omega_{IIC,(i,q+1) \rightarrow (j,q),\zeta}$$

Where the energies are $E_{ij,q} = I_q - E_{i,q} + E_{j,q+1}$.

Inverse charge transfer: Detailed balance

Again, the detailed balance equations are found considering the microscopic reversibility of the atomic processes. The inverse process of the charge transfer consist in the target capture of bound electrons from the projectile ions. Therefore, the inverse charge transfer can be found through the expression:

$$n_{i,q}^P n_{l,\zeta}^T \omega_{CT,(i,q) \rightarrow (j,q-1)} = n_{j,q-1}^P n_{m,\zeta+1}^T \omega_{ICT,(j,q-1) \rightarrow (i,q)}$$

Then using the Saha-Boltzmann equation, with some straightforward manipulations, the inverse charge transfer is expressed as:

$$\omega_{ICT,(i,q) \rightarrow (j,q+1)} = \frac{g_{l,\zeta}^T g_{i,q+1}^P e^{-E_{ji,q}/kT}}{g_{m,\zeta+1}^T g_{j,q}^P e^{-E_{lm,\zeta}/kT}} \cdot \omega_{CT,(i,q) \rightarrow (j,q-1)}$$

Where the energies are $E_{ji,q} = I_q - E_{j,q} + E_{i,q+1}$ and $E_{lm,\zeta} = I_\zeta - E_{l,\zeta} + E_{m,\zeta+1}$.

Bibliography

- [1] Anthony L Peratt. Advances in numerical modeling of astrophysical and space plasmas. In *Advanced Topics on Astrophysical and Space Plasmas*, pages 92–163. Springer, 1997.
- [2] Claude Deutsch and Gilles Maynard. Ion stopping in dense plasmas: A basic physics approach. *Matter and Radiation at Extremes*, 1(6):277–307, 2016.
- [3] Gilles Maynard. Interaction of heavy ions beams with hot and dense plasmas. application to inertial fusion. 1987.
- [4] Günter Zwicknagel, Christian Toepffer, and Paul-Gerhard Reinhard. Stopping of heavy ions in plasmas at strong coupling. *Physics reports*, 309(3):117–208, 1999.
- [5] Witold Cayzac. *Ion energy loss at maximum stopping power in a laser-generated plasma*. PhD thesis, Université Sciences et Technologies-Bordeaux I, 2013.
- [6] TA Mehlhorn. Finite material temperature model for ion energy deposition in ion-driven icf targets. Technical report, Sandia National Labs., Albuquerque, NM (USA), 1980.
- [7] Thomas Peter. T. peter and j. meyer-ter-vehn, *phys. rev. a* 43, 1998 (1991). *Phys. Rev. A*, 43:1998, 1991.
- [8] OR Gasparyan, S Yu Gus'kov, DV Il'in, VE Sherman, and NV Zmitrenko. Mathematical modeling of the heating of a fast ignition target by an ion beam. *Journal of Russian Laser Research*, 34(1):33–40, 2013.
- [9] David Salzmänn. *Atomic physics in hot plasmas*, volume 97. Oxford University Press on Demand, 1998.
- [10] Leonhard Euler. *Institutionum calculi integralis*. 1768.
- [11] Uri M Ascher and Linda R Petzold. *Computer methods for ordinary differential equations and differential-algebraic equations*, volume 61. Siam, 1998.
- [12] Marsha J Berger and Phillip Colella. Local adaptive mesh refinement for shock hydrodynamics. *Journal of computational Physics*, 82(1):64–84, 1989.

- [13] G Espinosa, R Rodríguez, JM Gil, F Suzuki-Vidal, SV Lebedev, A Ciardi, JG Rubiano, and P Martel. Influence of atomic kinetics in the simulation of plasma microscopic properties and thermal instabilities for radiative bow shock experiments. *Physical Review E*, 95(3):033201, 2017.
- [14] David Casas, Alexander A Andreev, Matthias Schnürer, Manuel D Barriga-Carrasco, Roberto Morales, and Luis González-Gallego. Stopping power of a heterogeneous warm dense matter. *Laser and Particle Beams*, 34(2):306–314, 2016.
- [15] Bin He and Jian-Guo Wang. Investigation of stopping power for deuterons in partially ionized warm al plasmas. *Physics of Plasmas*, 21(6):063111, 2014.
- [16] DB Zou, LX Hu, WQ Wang, XH Yang, TP Yu, GB Zhang, JM Ouyang, FQ Shao, and HB Zhuo. Tunable proton stopping power of deuterium-tritium by mixing heavy ion dopants for fast ignition. *High Energy Density Physics*, 18:1–6, 2016.
- [17] S Yu Gus'kov, DV Il'in, J Limpouch, O Klimo, and VE Sherman. Parameters of an ion beam and characteristic features of its slowing-down in a plasma during fast ignition of an inertial fusion target. *Plasma Physics Reports*, 36(6):473–481, 2010.
- [18] FC Young, D Mosher, SJ Stephanakis, Shyke A Goldstein, and TA Mehlhorn. Measurements of enhanced stopping of 1-mev deuterons in target-ablation plasmas. *Physical Review Letters*, 49(8):549, 1982.
- [19] BL Moiseiwitsch. Relativistic second-order oppenheimer-brinkman-kramers cross sections for electron capture. *Physical Review A*, 39(11):5609, 1989.